

Article

Human Serum Albumin Grafted by Monomeric and Polymeric β -Cyclodextrin as Drug Delivery System for Levofloxacin with Improved Pharmacological Properties

Tatiana Yu Kopnova , Linara R. Yakupova , Natalya Georgievna Belogurova
and Elena Vadimovna Kudryashova * 

Chemistry Department, Lomonosov Moscow State University, 119991 Moscow, Russia

* Correspondence: helena_koudriachova@hotmail.com

Abstract: Human serum albumin (HSA) is a multifunctional protein, known to be a natural carrier for a number of endogenous and exogenous compounds, including drugs. HSA-based drugs formulation is a clinically validated approach to improve pharmacological properties and biodistribution (such as in Abraxane). Based on this, one might like to modify HSA in a way that its distribution is more favorable for certain therapeutic purposes. Levofloxacin (LV), a broad-spectrum antibiotic drug, could benefit from extended systemic exposure, and stronger interactions with plasma proteins could be useful for this purpose. We engrafted monomeric or polymeric cyclodextrins (CDs) on the surface of HSA molecules to strengthen the LV adsorption (the CD–LV dissociation constant is three orders of magnitude lower than that of HSA–LV). We found that (HSA–HPolS)_{conj}+LV exhibited the highest activity against *E. coli*, whereas (HSA–HPCD)_{conj}+LV was the most effective against *B. subtilis*, and both HSA conjugates were more potent than LV alone or LV with HSA. Further fine-tuning of HSA could yield an improvement in biodistribution and thus a more favorable risk/benefit ratio.

Keywords: levofloxacin; human serum albumin; hydroxypropyl- β -cyclodextrin; conjugate; drug delivery systems; antibacterial activity



Citation: Kopnova, T.Y.; Yakupova, L.R.; Belogurova, N.G.; Kudryashova, E.V. Human Serum Albumin Grafted by Monomeric and Polymeric β -Cyclodextrin as Drug Delivery System for Levofloxacin with Improved Pharmacological Properties. *Future Pharmacol.* **2024**, *4*, 139–162. <https://doi.org/10.3390/futurepharmacol4010010>

Academic Editors: Fabrizio Schifano and Ali Zarrabi

Received: 5 November 2023

Revised: 4 December 2023

Accepted: 8 February 2024

Published: 13 February 2024



Copyright: © 2024 by the authors. Licensee MDPI, Basel, Switzerland. This article is an open access article distributed under the terms and conditions of the Creative Commons Attribution (CC BY) license (<https://creativecommons.org/licenses/by/4.0/>).

1. Introduction

Blood contains essential drug-binding proteins such as human serum albumin (HSA) and acid glycoprotein as well as lipoproteins and erythrocytes [1,2]. The binding of drugs to HSA and acid glycoprotein has been extensively studied over the past few decades. HSA holds a preeminent position as one of the most abundant and compact proteins within blood plasma. HSA has eight binding sites, which can bind to both endogenous and xenobiotic compounds with varying affinities [3]. However, two major sites of HSA are primarily involved in ligand binding and exhibit a preference for acidic drugs. These two sites are also known as Sudlow site I (warfarin-azapropazone site) and Sudlow site II (indole-benzodiazepine site) [4]. Despite its large size, HSA is not limited to plasma but is distributed extravascularly, similar to acid glycoprotein [2]. HSA plays a pivotal role in transporting a wide array of metabolic compounds and therapeutic drugs. For example, HSA exhibits an intriguing ability to bind with albumin-binding proteins, particularly membrane-associated gp60 (albondin) and its secreted protein that is acidic and rich in cysteine (SPARC) [5,6]. Albondin receptors, residing on the endothelial cells of tumor blood vessels, facilitate the transcytosis of albumin across continuous endothelial barriers. HSA's exceptional properties extend beyond its role as a transport protein, and it has emerged as a promising candidate for gene therapy due to its remarkable ability to avoid unwanted interactions with serum components. Therefore, the formation of a drug-HSA complex can significantly impact the bioactivity and bioavailability of drugs [3,7].

Levofloxacin (LV) stands out as a highly esteemed antibacterial agent with a broad spectrum of applications in the treatment of various diseases rooted in bacterial infections [8–10]. While

LV demonstrates good efficiency, prolonged therapeutic regimens can give rise to adverse effects including bacterial resistance. Thus, it becomes imperative to devise drug delivery systems aimed at mitigating potential side effects. Cyclodextrins are widely used for this purpose [11].

Cyclodextrins (CDs) are cyclic oligosaccharides that have gained widespread recognition in the field of pharmacology due to their remarkable ability to enhance the bioavailability and pharmacokinetics of inherently soluble yet lipophilic drugs [11–13]. Among these, hydroxypropyl- β -cyclodextrin (HPCD) holds a prominent position as a highly soluble and easily synthesized CD. We have previously reported that LV forms a remarkably stable complex with HPCD, characterized by an association constant of $(1.0 \pm 0.3) \times 10^3 \text{ M}^{-1}$ [14].

To achieve more substantial effects, we proposed the use of macromolecules constructed from CDs covalently linked to one another [15,16]. In this study, our focus was on investigating the complexation of LV with a polymer synthesized through the crosslinking of HPCD tori with succinic acid (HPolS), denoted as LV+HPolS. Detailed descriptions of these complexes can be found in our previous publications. The LV+HPolS complex exhibits an association constant of $(2.2 \pm 0.4) \times 10^5 \text{ M}^{-1}$ [16].

Human serum albumin (HSA) is a crucial blood plasma protein with multifaceted functions, including the maintenance of osmotic pressure, pH buffering, and the transport of diverse substances [17]. Furthermore, HSA plays a pivotal role in shaping the pharmacokinetic and biodistribution profiles of drug molecules. Hence, it is promising to devise drug delivery systems that leverage the modulatory potential of HSA in these physiological processes [3].

In our current study, we embark on the creation of novel drug delivery systems for levofloxacin (LV) using HSA grafted with monomeric or polymeric HPCD. These innovative developments hold great promise, primarily owing to their non-cytotoxic nature and the capacity for prolonged circulation within the bloodstream. So, we synthesize three types of HSA-based particles: complexes of LV with (HSA–HPCD) and (HSA–HPolS) conjugates in comparison with conjugates of non-grafted HSA–LV. Here, we study the molecular details of the HSA grafting by monomeric or polymeric HPCD (HSA–HPCD)_{conj} and (HSA–HPolS)_{conj} and its influence on the interaction of HSA with LV. We also seek to investigate how the creation of such systems would impact the physico-chemical properties and antibacterial efficacy of levofloxacin (LV) concerning both Gram-positive (*Bacillus subtilis*) and Gram-negative (*Escherichia coli*) bacterial cells.

2. Materials and Methods

2.1. Materials

Levofloxacin (LV), 2-hydroxypropyl- β -cyclodextrin (HPCD) with a hydrogen substitution degree of 1–1.3 in one D-glucopyranose link, succinic anhydride, and human serum albumin (HSA), Woodward's reagent, carbonyldiimidazole, and 2-(N-morpholino)ethanesulfonic acid (MES) were acquired from Sigma-Aldrich (St. Louis, MO, USA).

2.2. Methods

2.2.1. Synthesis of HPCD-Based Polymer Linked by Succinic Anhydride (HPolS)

In this study, polymers based on HPCD linked by succinic anhydride were synthesized according to the procedure outlined in reference [15]. Briefly, a specified amount of HPCD solution ($C = 60 \text{ mg/mL}$) was heated at $100 \text{ }^\circ\text{C}$ in the presence of NaH_2PO_4 . Subsequently, the linker's aqueous solution (3 M succinic anhydride) was added dropwise to the reaction mixture, which was stirred for 1.5 h. The molar ratio of HPCD to linker was maintained at 1:15.

The obtained polymer, referred to as HPolS, was purified through dialysis using a membrane with a molecular weight cut-off of 12 kDa (Serva, Heidelberg, Germany). The purified polymer was then dried for 24 h at $37 \text{ }^\circ\text{C}$.

The concentration of cyclodextrin (CD) torus in HPolS was determined using FTIR spectroscopy, specifically by analyzing the 1032 cm^{-1} band corresponding to the C–O–C bond in the CD torus. Calibration dependence was established for accurate concentration determination.

2.2.2. Synthesis of HSA Conjugates with HPCD or HPolS

To obtain conjugates of HSA with HPCD or HPolS, in the first stage, the hydroxyl groups in the ligands were activated using carbonyldiimidazole (CDI). Then, 120 μL of ligands (a 0.1 M solution of HPCD or a 0.065 M solution of HPolS) and 900 μL of a 0.04 M CDI solution were mixed with 4.980 mL of a PBS buffer. The solutions were incubated at room temperature and constantly stirred for 2 h. Then, 2 mL of a 0.4 mM solution of HSA was added to each sample and mixed at room temperature for 12 h. In the last stage, the conjugates were washed from unreacted reagents by dialysis (cut-off molecular weight 3.5 kDa membrane, Serva, Heidelberg, Germany) and lyophilized. Atomic force microscopy (AFM microscope NTEGRA II) was used to visualize the polymeric particles of HSA Conjugates with HPCD or HPolS and compare it in terms of shape and size with non-modified HPolS.

2.2.3. Synthesis of HSA Conjugates with LV

To obtain protein conjugates with LV, the carboxyl group of the drug was previously activated with Woodward's reagent (WRK). For this, 300 μL of the LV solution ($C_{\text{LV}} = 8 \text{ mM}$ in MES, $\text{pH} = 5.0$) was added to 600 μL of WRK solution ($C_{\text{WRK}} = 12 \text{ mM}$, $\text{pH} = 3.5$) and 5 mL MES buffer solution, and the reaction mixture was incubated at room temperature while constantly being stirred for 2 h. The molar ratio of the components in the reaction was 1:3 for LV:WRK. After that, to 2 mL of the resulting solution, the HSA solution ($C_{\text{HSA}} = 0.08 \text{ mM}$ in a PBS buffer solution, $\text{pH} = 7.4$) was added in a volume of 2 mL and incubated at room temperature while constantly being stirred for 3 h. The mole ratios of LV:HSA were 1:5 and 1:10. Finally, both conjugates were washed from unreacted reagents by dialysis (cut-off molecular weight 3.5 kDa membrane) and lyophilized.

2.2.4. Obtaining Non-Covalent Complexes with LV

Non-covalent conjugate complexes with LV were obtained by mixing the solutions of LV and $(\text{HSA-HPCD})_{\text{conj}}$ or $(\text{HSA-HPolS})_{\text{conj}}$ in a molar ratio of 1:1 for LV:CD_{tori} in a sodium-phosphate buffer solution and incubating at 37 °C for 40 min.

2.2.5. UV-Vis Spectrophotometry

UV spectra were acquired utilizing the Ultrospec 2100 Pro apparatus procured from Amersham Biosciences, San Francisco, CA, USA. Absorption spectra for LV, WRK, and their mixture were recorded using a quartz cell with an optical path length of 1 cm, sourced from Hellma Analytics, Jena, Germany, encompassing the spectral range spanning from 200 to 450 nm.

2.2.6. FTIR Spectroscopy

FTIR spectra of the sample solutions were acquired using the FTIR microscope MICRAN-3 (Novosibirsk, Russia) and a Bruker Tensor 27 spectrometer (Ettlingen, Germany) equipped with an attenuated total reflection cell with a ZnSe single-reflection crystal. Spectra were recorded within the wavenumber range of 2500–900 cm^{-1} with a 1 cm^{-1} resolution, averaging 3 measurements of 70 scans each. Data analysis was conducted using Opus 7.0 software.

The assessment of secondary structural components in the samples containing albumin was accomplished through an in-depth analysis of the FTIR spectra within the spectral region spanning from 1700 to 1600 cm^{-1} . The primary spectral bands were meticulously identified through the application of the second derivative technique, followed by spectrum deconvolution employing the Levenberg–Marquardt algorithm.

2.2.7. Circular Dichroism Spectroscopy

Circular dichroism (CD) spectra were recorded using the J-815 spectrometer by Jasco (Tokyo, Japan).

The experimental measurements were executed at a temperature of 25 °C employing quartz cuvettes with a path length of 1 mm. The wavelength range covered spanned from 200 to 260 nm. Spectra were obtained through five scans at 1 nm intervals, with the HSA concentration maintained at 0.02 mM. The content of secondary structures, the obtained spectra were subjected to analysis using the CDNN program, Version 2. Each experiment was repeated three times, and the results were reported with a standard deviation (SD) of 3 (n = 3).

2.2.8. Fluorescence Spectroscopy

Fluorescence measurements were performed using the Varian Cary Eclipse spectrophotometer, manufactured by Agilent Technologies (Santa Clara, CA, USA). The emission spectra of HSA were recorded under controlled conditions at 37 ± 0.1 °C. A 10 mm quartz cuvette was employed for the measurements, and the excitation wavelength was set at 280 nm. The emission scans were conducted with a 1 nm step within the wavelength range of 290–550 nm. It is noteworthy that the protein concentration was consistently maintained at 0.02 mM using a PBS buffer solution at a pH of 7.4.

To assess the quenching of protein fluorescence by small molecules, we applied the Stern–Volmer Equation (1). This equation takes into account both statistical and dynamic quenching effects [18].

$$F_0/F = 1 + K_{SV}[Q] = 1 + k_q\tau_0[Q], \quad (1)$$

This equation incorporates F_0 and F , denoting the fluorescence intensities in the absence and presence of a drug form acting as a quencher. Within its framework, K_{SV} takes on the role of the Stern–Volmer constant, $[Q]$ signifies the molar concentration of the quencher, k_q characterizes the bimolecular constant governing quenching rate, and τ_0 corresponds to the lifetime of HSA's fluorescence in the absence of the quencher. To ascertain the binding constant (K_a) of HSA to the drug form and the number of binding sites (n), Equation (2) was employed under controlled temperature conditions:

$$\lg \frac{F_0 - F}{F} = \lg K_a + n \lg [Q]. \quad (2)$$

We calculated thermodynamic parameters, including the Gibbs free energy change (ΔG), enthalpy change (ΔH), and entropy change (ΔS) of the reaction using the Van't Hoff Equations (3)–(5):

$$\Delta G = -RT \ln K_a \quad (3)$$

$$\Delta G = \Delta H - T\Delta S \quad (4)$$

$$\ln K_a = \frac{\Delta S}{R} - \frac{\Delta H}{RT} \quad (5)$$

where R is universal gas constant, and T is the temperature.

2.2.9. Release Kinetic Studies

The release of LV was investigated using a dialysis method. Specifically, 2 mL of the sample was placed in a dialysis bag with a molecular weight cutoff (MWCO) of 3.5 kDa (Orange Scientific, Braine-l'Alleud, Belgium). The entire system was incubated at 37 °C with gentle agitation at 150 rpm, and UV or fluorescence spectra of the external solution were recorded over time.

The experiment considered 100% of LV as released when the concentration of LV inside the dialysis bag equaled the concentration of LV in the external solution, representing 50% of the initial LV's concentration.

2.2.10. Evaluation of Antibacterial Activity In Vitro Studies

In this investigation, two bacterial strains, namely *Escherichia coli* (ATCC 25922) and *Bacillus subtilis* (ATCC 6633), sourced from the National Resource Center's Russian collection of industrial microorganisms at the SIC "Kurchatov Institute", were utilized.

These strains were cultured for a period of 18–20 h at 37 °C to attain a concentration of approximately 2×10^8 colony-forming units per ml (CFU/mL), a quantification method based on A_{600} measurements, in the liquid nutrient medium Luria–Bertani (LB) (pH 7.2). It is noteworthy that *E. coli* cultures were cultivated without agitation, while *B. subtilis* cultures were stirred at 170 rpm.

For the microbiological tests, the suspensions of the bacterial cultures were standardized to a 0.5 McFarland standard, resulting in a CFU concentration of approximately 0.3×10^8 (CFU) in the liquid LB nutrient medium (pH 7.2). Subsequent experiments in the liquid medium involved adding 100 μ L of the test samples (the concentration of LV in each sample was 10 ng/mL or 50 ng/mL) to 5000 μ L of the bacterial cultures. These samples were then incubated at 37 °C for a duration of four days. At specific time points, 100 μ L from each sample was extracted and diluted with PBS. Subsequently, the absorbance was measured at 600 nm, with concurrent CFU controls.

To quantitatively assess the relationship between CFU (cell viability) and the concentration of LV, 50 μ L of each sample was diluted in the range of 10^6 – 10^8 times and plated on Petri dishes. These Petri dishes were subsequently incubated at 37 °C for 24 h, after which the number of colonies (CFU) was determined.

We determined the minimum inhibition concentration (MIC) using the agar well diffusion method [19–21]. The cell suspension of overnight-cultured *Escherichia coli* (ATCC 25922) and *Bacillus subtilis* (ATCC 6633) (grown in the Luria–Bertani medium for 12 h) was diluted to a 0.5 McFarland standard. Four wells with diameters of 9 mm were created in the agar using sterile plastic pipette tips after evenly distributing bacteria over the agar surface. Subsequently, 50 μ L of the samples (including sterile buffer as the negative control; LV, (HSA–HPCD)_{conj}+LV, and (HSA–HPoIS)_{conj}+LV with C_{LV} concentrations of 1, 2, 5 μ g/mL; and for (HSA–LV)_{conj} 1:5 and (HSA–LV)_{conj} 1:10 concentrations of LV were 10.0, 20.0, 50.0 μ g/mL for each sample) were placed in the wells. The Petri dishes containing the samples were then incubated at 37 °C. After 24 h, the diameters of the inhibition zones were analyzed.

MICs were determined as the concentration of the sample at which the absence of bacterial growth equaled that of the removed agar (with a diameter of approximately 9 mm) using the following Equation (6):

$$\lg C = a \times S_{inh} + \lg MIC \quad (6)$$

where C is the concentration of LV (μ g/mL), S_{inh} is the square of the inhibition zone (mm^2), and a is a constant. Each sample was tested in triplicate, and the data are presented with standard deviations.

2.2.11. Hemolysis Assay

The hemolysis ratios for the conjugates were assessed using purified erythrocytes obtained voluntarily from one of the authors. Initially, 3 mL of blood, stored in a tube with 0.3 mL 2% EDTA, underwent centrifugation at 1000 rpm for 10 min. The erythrocyte mass was subsequently washed with 0.15 M NaCl solution and centrifuged through four repetitions of this process. Following this, 40 μ L of the erythrocyte suspension in 0.15 M NaCl was combined with 40 μ L of the conjugate solution in the same saline solution, each at varying concentrations (final concentrations: 0.17, 1.70, and 3.30 mg/mL for each conjugate).

For the negative control representing 100% hemolysis, 6 μ L of 2% Triton X-100 was added to a 200 μ L erythrocyte solution. Conversely, for the positive control signifying 0% hemolysis, 40 μ L of the saline solution was added. The samples were incubated for 2 h at 37 °C and subsequently centrifuged at 1000 rpm for 10 min. The absorbance of the supernatant solutions was measured using a UV spectrophotometer at a wavelength of 540 nm to quantify the released hemoglobin. The hemolysis ratios were calculated using Equation (7):

$$\text{Hemolysis ratio}(\%) = \frac{A(\text{sample}) - A(\text{positive})}{A(\text{negative}) - A(\text{positive})} \times 100 \quad (7)$$

3. Results and Discussion

The formation of LV+HPCD or LV+HPolS complexes is advantageous in enhancing solubility and extending the duration of LV's therapeutic action. However, cyclodextrins (CDs) can partially shield LV's binding sites on HSA. To achieve more significant enhancements in LV's pharmacodynamic and pharmacokinetic attributes, in this work, we developed a new drug delivery system based on the HSA grafted with monomeric or polymeric HPCD.

For synthesis of the conjugates with HSA (HSA grafted with CDs), we used 2-hydroxypropyl- β -cyclodextrin (HPCD) since this substance is able to form quite stable inclusion complexes via the «guest-host» mechanism with LV ($K_{a(LV+HPCD)} = (1.0 \pm 0.3) \times 10^3 \text{ M}^{-1}$) [14]. The formation of the HPCD+LV non-covalent complex affects the physicochemical parameters of the drug [12]. Previously, we have shown that the polymers based on CDs have a more significant effect on LV's biopharmaceutical properties, enhancing its antibacterial properties, solubility and bioavailability. So, we used a polymer based on HPCD (the polymer—HPolS), which shows a number of improved properties, such as higher association constant $K_{a(LV+HPolS)} = (1.0 \pm 0.1) \times 10^6 \text{ M}^{-1}$, prolonged action, and increasing of antibacterial activity. Polymer synthesis was carried out according to our previous article [15], and succinic anhydride was used as a linker since it is a biocompatible bifunctional crosslinking agent. The hydrodynamic diameter of polymer nanoparticles is 200 nm, and the ζ -potential is -0.6 mV (Table 1).

Table 1. Physicochemical properties of non-covalent complexes of LV and CDs.

Parameter	HPCD	HPolS
ζ -potential, mV	0	-0.6 ± 0.02
Hydrodynamic radius, nm	0.15	200 ± 20
K_a with LV, M^{-1}	$(1.0 \pm 0.3) \times 10^3$	$(1.0 \pm 0.1) \times 10^6$

3.1. Synthesis of HSA Grafted by Monomeric and Polymeric HPCD

The synthesis of HSA conjugates with HPCD or HPolS was initiated by the activation of the hydroxyl group in the ligand using carbonyl diimidazole (CDI) (Figure 1). CDI forms highly reactive imidazolyl-carbamate intermediates upon reaction with alcohols. The imidazolyl-carbamate group is highly electrophilic and readily undergoes nucleophilic attacks by a variety of nucleophiles, including amines, thiols, and carboxylic acids, leading to the formation of amides, thioesters, and esters with high yields [22–24]. In the second stage, the HSA was added, which reacted with the activated ligand due to the high content of lysine residues. As a result, conjugates with a covalent urethane bond were obtained— $(\text{HSA-HPCD})_{\text{conj}}$ and $(\text{HSA-HPolS})_{\text{conj}}$ —the formation of which was monitored using FTIR.

To improve the biopharmaceutical characteristics of the LV, in this study, we synthesized conjugates of the LV with HSA with a high degree of the drug's inclusion. Two types of HSA conjugates with LV were obtained with a covalent and non-covalent bond between the protein and the drug molecule. In the first case, a covalent bond was formed between the carboxyl group of LV and the amino group of lysine residues of the protein (Figure 2A). To form this, in the first stage, the activation of the carboxyl group was carried out using Woodward reagent (WRK), which is an isoxazolium salt that causes a specific and rapid modification of carboxylic groups in various molecules [25]. Initially, this reagent was developed for the synthesis of peptides [26], but now it is used to activate carboxyl groups in various compounds [27]. In the next stage, a HSA's solution was added to the activated LV molecule, resulting in an amide bond between the protein and LV.

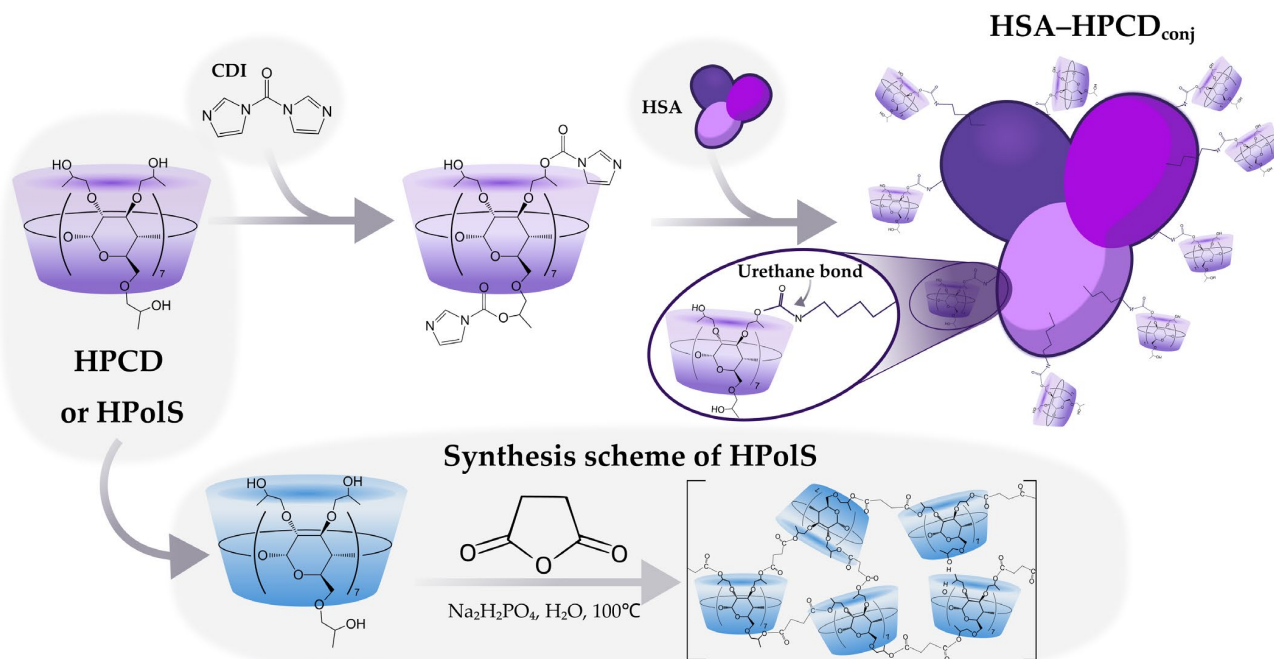


Figure 1. The scheme of conjugates' synthesis of 2-hydroxypropyl- β -cyclodextrin (HPCD) or polymer based on HPCD (HPols) with human serum albumin (HSA), PBS, pH = 7.4, T = 22 °C.

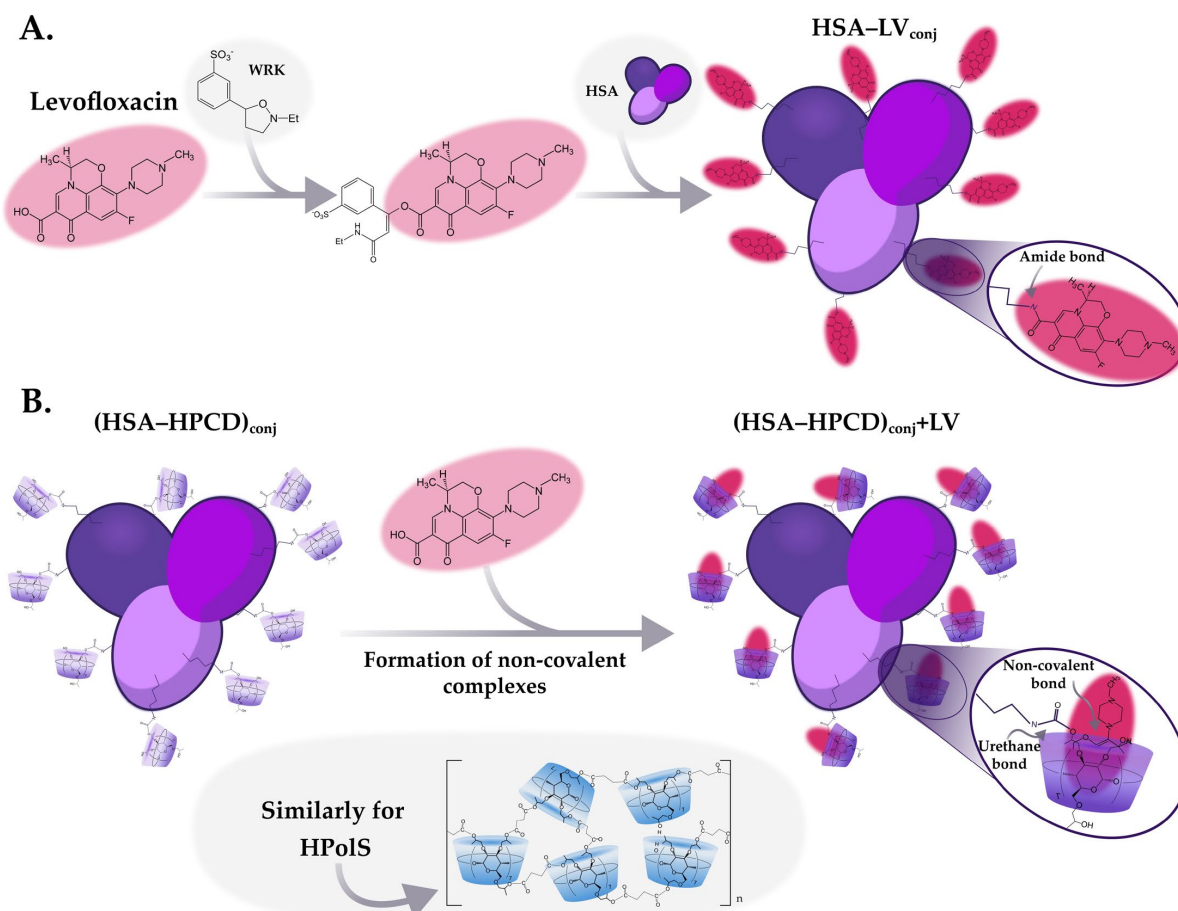


Figure 2. (A) The scheme of conjugates' synthesis levofloxacin (LV) with HSA; (B) The scheme of synthesis of non-covalent complexes LV with conjugates, PBS, pH = 7.4, T = 22 °C.

Upon the reaction of LV with WRK, a novel absorption peak emerged in UV spectrum around 345 nm. This spectral feature may serve as an indication of the formation of a stable enol ester bond, resulting from the modification of LV's carboxylate group by the WRK [28,29]. Remarkably, this peak exhibited substantial augmentation within the initial twenty minutes of the experiment. However, beyond the 20 min mark, no significant changes were observed in this band. So, the conjugation reaction was completed. Our scrutiny of the UV spectra over a 2 h period unveiled a gradual diminishment of the 290 nm band (assigned to WRK), indicative of the hydrolysis of WRK [30].

For the second system, non-covalent LV complexes were obtained with the conjugates HSA–HPCD_{conj} and HSA–HPoIS_{conj} described above (Figure 2B). Cyclodextrins are able to form inclusion complexes with large binding constants of $\sim 10^4$ – 10^6 M⁻¹ [31,32] and non-covalent complexes with antibacterial molecules. One may expect that the formation of non-covalent complexes between LV and (HSA–HPCD)_{conj} or (HSA–HPoIS)_{conj} (Figure 2B) would exhibit high binding affinities. The binding constants for these systems were subsequently calculated through fluorescence spectroscopy analysis and are thoroughly discussed in the next section.

3.2. FTIR and Structure Features of Synthesized Molecules

Figure 3a,b provides a visualization of the FTIR spectra for the conjugates HSA–HPoIS and HSA–HPCD in comparison with free HSA, HPCD, and HPoIS. The cross-linking between HSA and HPoIS or HPCD involves the formation of carbamate (urethane) bonds. These bonds appeared between lysine (Lys) residues in HSA and hydroxyl groups within the CDs activated using CDI.

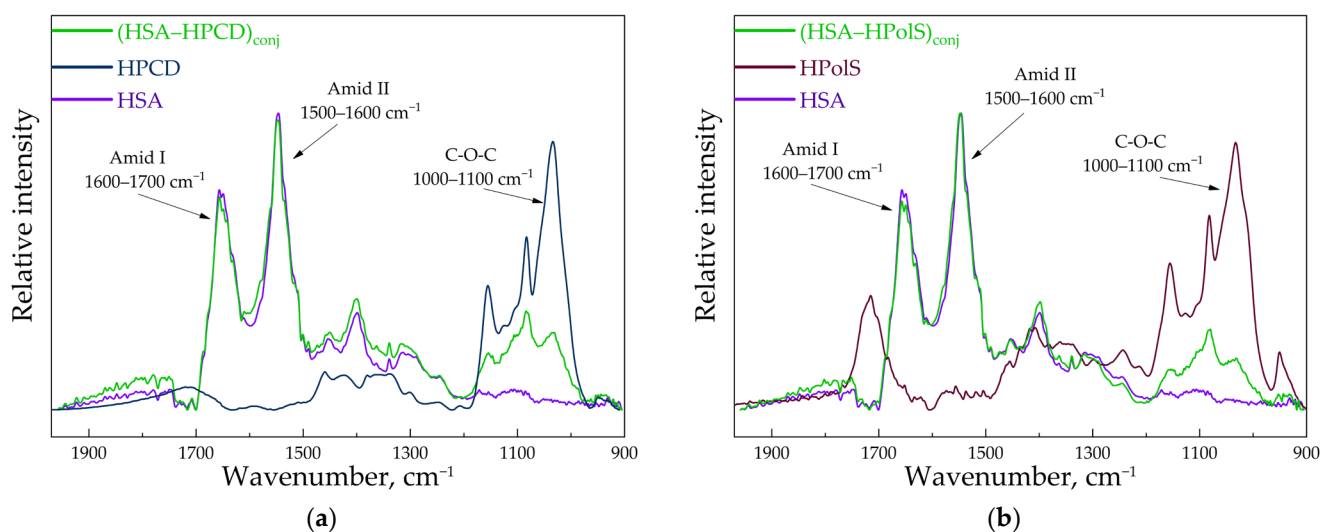


Figure 3. (a) The FTIR spectra of HSA, (HSA–HPCD)_{conj}, and HPCD at $C_{\text{HSA}} = 0.1$ mM, $C_{\text{HPCD}} = 1.5$ mM H₂O, pH 7.0, 22 °C; (b) The FTIR spectra of HSA, (HSA–HPoIS)_{conj}, and HPoIS at $C_{\text{HSA}} = 0.1$ mM, $C_{\text{HPoIS}} = 1.5$ mM H₂O, pH 7.0, 22 °C.

Notably, carbamate bonds manifest distinctive peaks in the FTIR spectra, specifically the C–N and C–O stretching modes, observed at 1076 cm⁻¹ and 1024 cm⁻¹, respectively. Additionally, the presence of a shoulder peak at 1069 cm⁻¹ is likely attributed to the second C–N stretching mode. Furthermore, carbamate bonds are anticipated to exhibit characteristic vibration modes at 1645 cm⁻¹ and 1600 cm⁻¹, specifically related to N–H rocking [33–35].

Upon examination of the FTIR spectra for HSA–HPCD and HSA–HPoIS, the emergence of novel peaks indicative of carbamate bonds suggests the formation of covalent bonds between lysine (Lys) residues within HSA and hydroxyl groups present in the CDs during the synthesis process. In the FTIR spectra of the conjugates, we also observe distinc-

tive peaks related to bonds within HSA. Specifically, the amide I band ($1600\text{--}1700\text{ cm}^{-1}$) represents oscillations involving $\nu(\text{C}=\text{O})$ ($\sim 80\%$) and $\nu(\text{C}-\text{N})$ ($\sim 15\%$). Additionally, the amide II bands ($1500\text{--}1600\text{ cm}^{-1}$) correspond to $\delta(\text{N}-\text{H})$ ($\sim 60\%$), $\nu(\text{C}-\text{N})$ ($\sim 20\%$), and $(\text{C}-\text{C})$ ($\sim 10\%$) [36–38]. Furthermore, bands characteristic of oligosaccharides are evident in the conjugates. Prominent absorption bands in the range of $1100\text{--}1000\text{ cm}^{-1}$ were identified, corresponding to C–O–C glycoside bonds [39]. The formation of the HSA–HPOIS conjugate resulted in the appearance of bands at 1717 cm^{-1} and 1226 cm^{-1} , indicative of the presence of C=O in carboxylic and ester groups as well as C–O–C in ester groups, respectively [40].

The secondary structure of proteins is intricately linked to their biological functionality, which is a critical factor when proteins are employed as carriers for therapeutic drugs. The preservation of a protein’s biological activity is of paramount importance, particularly in the context of drug delivery, as it dictates the protein’s ability to interact with its intended targets. Previous studies have extensively documented alterations in the secondary structure of albumin as a consequence of complexation with various drugs [33,38–44]. In this research, we harnessed the power of FTIR spectroscopy to meticulously scrutinize these structural changes in albumin stemming from the creation of HSA conjugates with either HPCD or HPOIS. Our specific focus was channeled towards the examination of the amide I and amide II bands within the FTIR spectra, known for their heightened sensitivity to variations in the protein’s secondary structure.

Using deconvolution techniques on the amide I band, we extracted quantitative insights into the shifts in α -helices, β -structures, and random coils, shedding light on the nuanced alterations within HSA’s secondary structure (Figure 4a). Our findings revealed that the covalent binding between Lys residues in the HSA and hydroxyl groups in CD tori (the formation of $(\text{HSA}-\text{HPCD})_{\text{conj}}$ or $(\text{HSA}-\text{HPOIS})_{\text{conj}}$) did not induce significant structural deviations in HSA (Table 2). This observation negates the likelihood of aggregation events. The primary deviation detected was a minor increment in the content of a random coil in HSA’s secondary structure. We obtained the same results through the analysis of CD-spectra of HSA, $(\text{HSA}-\text{HPCD})_{\text{conj}}$, and $(\text{HSA}-\text{HPOIS})_{\text{conj}}$ (Figure 4b).

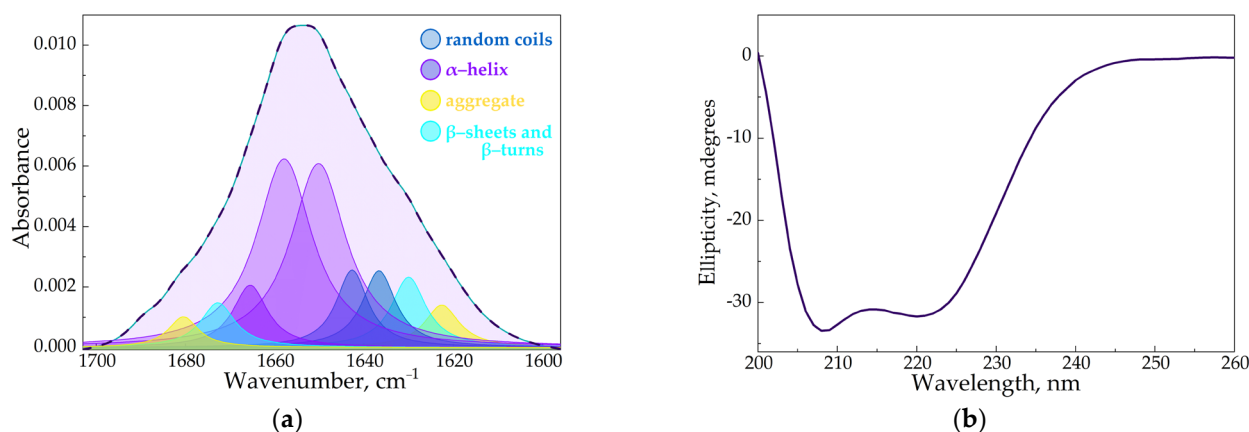


Figure 4. (a) An exploration into the deconvolution of HSA FTIR spectrum at $C_{\text{HSA}} = 0.06\text{ mM}$ (dark purple line) compared with the simulated spectrum portrayed using the dashed blue line, pH 7.4; (b) the resolute CD spectrum of HSA captured at $C_{\text{HSA}} = 0.02\text{ mM}$, pH 7.4.

Table 2. The content of secondary structures in HSA (from FTIR data): $C_{\text{HSA}} = 0.06\text{ mM}$, pH 7.4, SD ($n = 3$).

	α -Helix	β -Structures	Random
HSA	$64 \pm 2\%$	$19 \pm 1\%$	$17 \pm 1\%$
$(\text{HSA}-\text{HPCD})_{\text{conj}}$	$56 \pm 2\%$	$20 \pm 1\%$	$24 \pm 1\%$
$\text{HSA}-\text{(HPOIS)}_{\text{conj}}$	$54 \pm 2\%$	$20 \pm 1\%$	$26 \pm 1\%$

Vigilantly monitoring the secondary structure of proteins within drug delivery systems is of utmost importance, as it influences protein stability, drug loading and release, biocompatibility, functionality, quality control, formulation optimization, and overall safety and efficacy.

In the second systems where we aimed to form the conjugate of HSA and LV, we observed a noteworthy increase in the intensity of the amide I and amide II bands. This observation suggests that we successfully formed amide bonds between Lys residues within HSA and the carboxylic group of the LV in the conjugates (Figure 5).

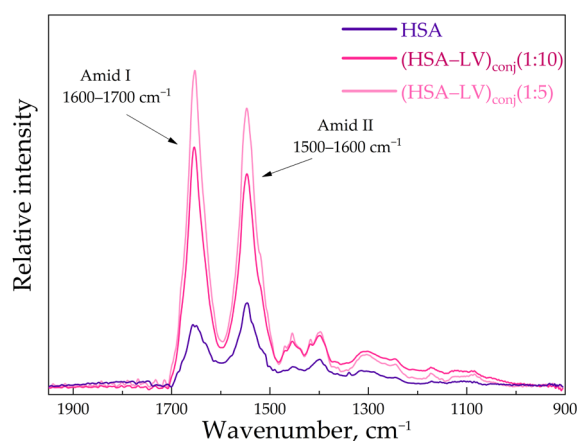


Figure 5. The FTIR spectra of HSA, $C_{\text{HSA}} = 0.02$ mM, $(\text{HSA-LV})_{\text{conj}} 1:10$ $C_{\text{HSA}} = 0.02$ mM, and $(\text{HSA-LV})_{\text{conj}} 1:5$ $C_{\text{HSA}} = 0.02$ mM, PBS, pH 7.4, 22 °C.

The reaction yield, as measured by HPCD/HPolS, denotes the percentage of HPCD tori in the $(\text{HSA-HPCD})_{\text{conj}}$ or $(\text{HSA-HPolS})_{\text{conj}}$ particles relative to the amount employed during the synthesis. HPCD's content was quantified using FTIR spectroscopy, with the intensity of the 1047 cm^{-1} absorption band corresponding to the oscillation of the C-O-C bond of the CD. In the case of $(\text{HSA-LV})_{\text{conj}}$, the reaction yield was determined by LV. LV's content was ascertained through FTIR spectroscopy, with the intensity of the 1490 cm^{-1} absorption band corresponding to the oscillation of the C-C_{aromatic} bonds of LV. Based on the analysis of the HSA conjugates using FTIR, it was found that the entire ligands (HPCD, HPolS or LV) were sewn to the protein globule during the synthesis reaction (Table 3).

Table 3. Physicochemical properties of conjugates of HSA and LV or CDs.

Parameter	$(\text{HSA-LV})_{\text{conj}} 1:5$	$(\text{HSA-LV})_{\text{conj}} 1:10$	$(\text{HSA-HPCD})_{\text{conj}}$	$(\text{HSA-HPolS})_{\text{conj}}$
Molecular weight, kDa	66.8	68.6	88.1	80.1
LV, % (w/w)	2.7%	5.4%	—	—
Molar ratio ¹	1:5	1:10	1:15	1:10

¹ Molar ratio of LV to HSA or CD torus to HSA.

3.3. Fluorescence Spectroscopy

For further elucidation of the molecular details, it is important to understand how CDs carriers would affect the binding of chemical fragments of LV with HSA. Moreover, we were interested in how the covalent that bound HPCD and HPolS to HSA would alter the thermodynamic parameters of HSA's interactions with LV.

Fluorescence is a valuable approach to studying the Trp-214 interaction of HSA with different molecule types since the fluorescence of Trp residues is sensitive to a protein's microenvironment. The measurement of intrinsic fluorescence quenching in proteins stands as a widely employed approach to unravel the intricate mechanisms underlying their interaction with ligands or drug molecules [41–43]. The detailed description of the interaction between LV and HSA has been previously elucidated [18,44,45]. In our previous works, we studied ternary systems where the drug is included in the complex

with monomeric or polymeric CDs [16,32,46,47]. Here, we studied the interactions of levofloxacin (LV) with HSA grafted with cyclodextrins (CDs) or CD polymers (CDPols).

3.3.1. Impact of HPCD, HPoIS, and Conjugate Formation on the Fluorescence Spectra of HSA and LV

We investigated the interaction between LV and HSA, LV+HPCD and HSA, LV+HPoIS and HSA, LV and (HSA-grafted-HPCD)_{conj}, and LV and (HSA-grafted-HPoIS)_{conj} using fluorescence spectroscopy. At an excitation wavelength of 280 nm, LV and HSA demonstrated distinct emission peaks at 456 and 340 nm, respectively (Figure ??a). HPCD and HPoIS had no signal under the present conditions.

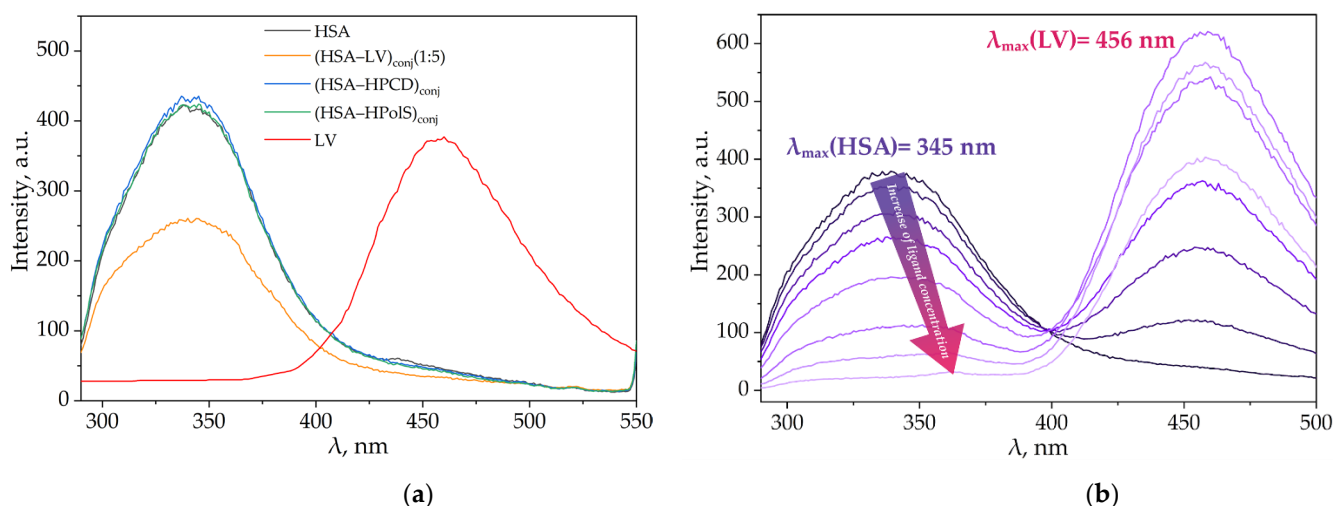


Figure 6. (a) Emission spectra of HSA (dark purple), (HSA–LV)_{conj} 1:5 (pink), (HSA–HPCD)_{conj} (light purple), and (HSA–HPoIS)_{conj} (green) with $\lambda_{ex} = 280$ nm, $C_{HSA} = 0.03$ mM, 37 °C, PBS, pH 7.4; (b) Fluorescence quenching of (HSA–HPCD)_{conj} by LV with $\lambda_{ex} = 280$ nm, $C_{HSA} = 0.03$ mM, 37 °C, PBS, pH 7.4.

In our previous studies, we reported that the formation of complexes between LV and HPCD, as well as the encapsulation of LV in HPoIS particles, led to a slight redshift of the emission maxima of the drug by 3–5 nm [16]. This shift signifies an augmentation in the hydrophilic nature of the microenvironment surrounding the drug, concomitant with a modest increase in the intensity of LV’s emission spectrum. Importantly, the presence of HPCD or HPoIS, even in concentrations up to 100 mM, did not exert a significant influence on the fluorescence properties of HSA [48].

The emission spectra of (HSA–HPCD)_{conj} and (HSA–HPoIS)_{conj} closely mirrored the emission profile of pure HSA (Figure ??a). This conformity suggests that this polysaccharide and oligosaccharide do not instigate substantial structural alterations or modifications in the fluorophores of HSA, thereby preserving its emission characteristics.

Most intriguingly, the formation of a conjugate between HSA and LV elicited profound spectral modifications. In particular, we noted a significant (two-fold) reduction in the intensity of HSA’s emission spectra (depicted by the pink curve in Figure ??a) compared to HSA alone at an equivalent concentration level (as shown by the purple curve in Figure ??a). Astonishingly, the formation of HSA–LV_{conj} resulted in the complete quenching of LV’s emission (as indicated by the absence of the LV peak in the pink curve, contrasting with the red curve representing LV alone at the same concentration). These observations offer compelling evidence of an alteration in the microenvironment surrounding LV.

We observed that an increase in the LV concentration in the presence of (HSA–HPCD)_{conj} or (HSA–HPoIS)_{conj} leads to a reduction in protein fluorescence, indicating a change in the microenvironment of Trp214 and the formation of a complex between LV and albumin (Figures 5b and ??a).

It is worth noting that the position of the protein emission peak shifts towards longer wavelengths, and the magnitude of this shift becomes stronger with higher concentrations of the quencher (e.g., with a molar excess of LV equal to five, the shift is approximately 20 nm). This suggests that the Trp214 residue experiences a less hydrophobic environment [44,45,49].

The determination of Stern–Volmer constants for the interactions between LV and $(\text{HSA-HPCD})_{\text{conj}}$ or $(\text{HSA-HPolS})_{\text{conj}}$ provides valuable insights (Figure 7b and Table S1). The obtained data suggest that the fluorescence quenching is primarily of a static nature. In other words, the quenching of fluorescence is mostly due to the formation of stable complexes between LV and $(\text{HSA-HPCD})_{\text{conj}}$ or $(\text{HSA-HPolS})_{\text{conj}}$.

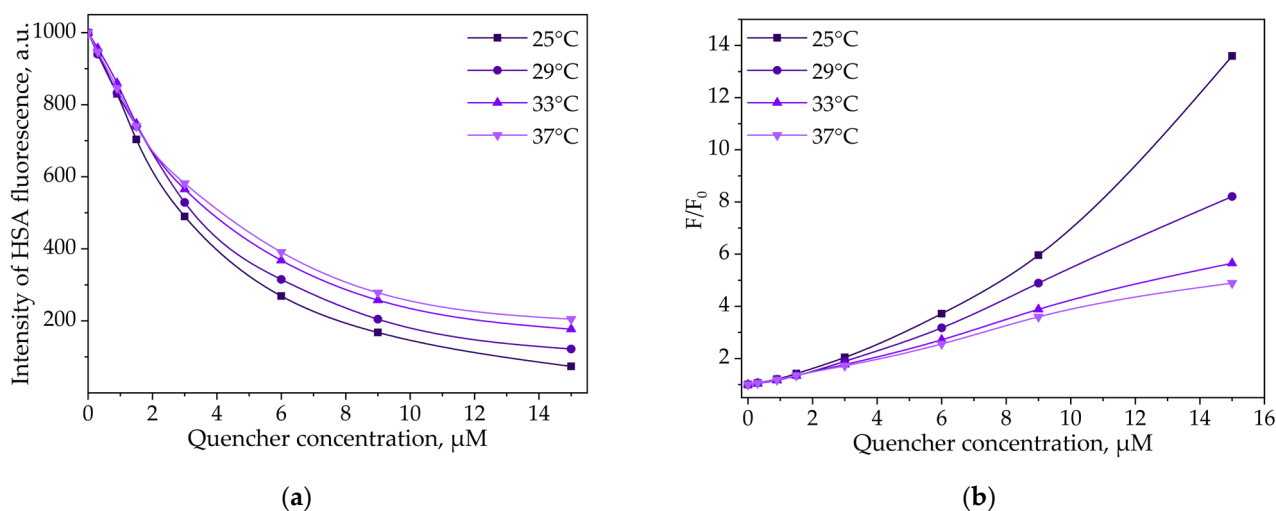


Figure 7. (a) The intensity of the $(\text{HSA-HPCD})_{\text{conj}}$ peak via the increase of the LV's concentration with $\lambda_{\text{ex}} = 280 \text{ nm}$, $C_{\text{HSA}} = 0.03 \text{ mM}$, 25–37 °C, PBS, pH 7.4; (b) Stern–Volmer dependences expressing the effect of $(\text{HSA-HPCD})_{\text{conj}}$ quenching via binding LV with $\lambda_{\text{ex}} = 280 \text{ nm}$, $C_{\text{HSA}} = 0.03 \text{ mM}$, 25–37 °C, PBS, pH 7.4.

Further investigation into the static quenching phenomenon under different conditions can yield important thermodynamic parameters. These parameters offer a deeper understanding of the energetics and stability of complex formation and shed light on the intricacies of drug–protein interactions.

3.3.2. Thermodynamic Parameters and Mechanisms of the Complex Formation of HSA and LV

Given the static nature of fluorescence quenching at low concentrations of LV, Equation (1) was modified into Equation (2), enabling the determination of binding constants (K_a) and stoichiometric coefficients (n). A noticeable reduction in both binding constant (K_a) and n was observed upon temperature variation. To gain a more comprehensive understanding of the overall process of complex formation between the antibacterial drug LV and $(\text{HSA-CD})_{\text{conj}}$, we proceeded to determine the associated thermodynamic parameters, as summarized in Table 4.

Consequently, the thermodynamic parameters of ΔH (enthalpy change), ΔS (entropy change), and ΔG (Gibbs free energy change) for the complexation reaction were determined using Equations (3)–(5), and the outcomes are detailed in Table 4. The primary forces driving the process of complex formation encompass the establishment of hydrogen bonds, electrostatic interactions, hydrophobic forces, and van der Waals interactions [50]. These interactions can either positively or negatively impact the changes in enthalpy (ΔH) and entropy (ΔS) [44,51–57]. The arrangement of the fluoroquinolone plays a crucial role in determining the primary forces involved in its interaction with HSA [44,52]. For example, Enrofloxacin engages in complex formation with HSA through hydrophobic interactions, resulting in positive values for both enthalpy and entropy changes. On the other hand,

Sparfloxacin and HSA exhibit a slightly negative ΔH and positive ΔS , indicating that electrostatic interactions play a primary role in the formation of the complex [44].

Table 4. Thermodynamic parameters of the interaction of human serum albumin with levofloxacin, pH 7.4 (CI = 0.95, n = 4, r = 0.999).

	T, K	n	$K_a, 10^5 \text{ M}^{-1}$	$\Delta G, \text{ kJ/mol}$	$\Delta H, \text{ kJ/mol}$	$\Delta S, \text{ J/mol/K}$
HSA+LV [32]	298	1.34 ± 0.07	23.4 ± 0.5	−36.3 ± 0.1	−57.7 ± 0.8	−71 ± 2
	302	1.33 ± 0.02	17.9 ± 0.3	−36.1 ± 0.1		
	306	1.32 ± 0.03	13.1 ± 0.4	−35.8 ± 0.1		
	310	1.33 ± 0.05	9.9 ± 0.2	−35.6 ± 0.1		
HSA+(LV+HPCD) [32]	298	1.51 ± 0.08	110 ± 1.2	−40.1 ± 0.2	−217.6 ± 1.4	−596 ± 4
	302	1.41 ± 0.04	34.0 ± 0.5	−37.7 ± 0.4		
	306	1.33 ± 0.03	12.6 ± 0.2	−35.7 ± 0.4		
	310	1.24 ± 0.03	3.5 ± 0.5	−32.9 ± 0.3		
(HSA+HPCD) _{conj} +LV	298	1.37 ± 0.01	17 ± 3	−35.6 ± 0.1	−187 ± 7	−510 ± 20
	302	1.29 ± 0.02	6 ± 1	−33.5 ± 0.1		
	306	1.23 ± 0.02	2.7 ± 0.7	−31.8 ± 0.1		
	310	1.12 ± 0.01	0.9 ± 0.1	−29.4 ± 0.1		
(HSA+HPolS) _{conj} +LV	298	1.21 ± 0.05	3.3 ± 1.9	−31.48 ± 0.3	−149 ± 8	−400 ± 20
	302	1.14 ± 0.05	1.4 ± 0.8	−29.73 ± 0.3		
	306	1.09 ± 0.02	0.68 ± 0.12	−28.33 ± 0.1		
	310	1.01 ± 0.04	0.31 ± 0.13	−26.68 ± 0.2		

HSA and LV Interactions

It was ascertained that the interaction between LV and HSA occurs spontaneously within the designated temperature range, as evidenced by the negative value of ΔG . The observation of negative values for ΔH and ΔS in the HSA+LV system suggests that complex formation is primarily driven by van der Waals forces and the establishment of hydrogen bonds. This finding aligns with similar conclusions reported in other works [18,44,52]. However, it is important to note that the ΔH , ΔS , and ΔG values calculated in our study are of the same order of the magnitude compared with the literature values for HSA and LV interactions (Table 5).

Table 5. Comparison of calculated and published thermodynamic parameters for the levofloxacin-human serum albumin system.

	T, K	n	$K_a, 10^5 \text{ M}^{-1}$	$\Delta G, \text{ kJ/mol}$	$\Delta H, \text{ kJ/mol}$	$\Delta S, \text{ J/mol/K}$
present study	310	1.33 ± 0.05	9.9 ± 0.2	−35.6 ± 0.1	−57.7 ± 0.8	−71 ± 2
present study ¹	298	1	0.6 ± 0.1	−27 ± 1	−38 ± 3	−37 ± 10
Zhang et al. ² [18]	298	1.04	0.49	−27.0	−42.2	−62.6
Zhang et al. ³ [18]				−27.4	−54.7	−91.6

¹ Calculation of thermodynamic parameters was made based on the equation: $\log(F_o - F)/F = \log K_a + \log[Q]$ and Equations (3)–(5) (n = 4, r = 0.987). ² Calculation using Equations (2)–(5) based on fluorescence spectroscopy data (r = 0.987). ³ Calculation based on affinity capillary electrophoresis data (r = 0.955).

Some discrepancy can be attributed to the assumption made by Zhang et al. regarding a 1:1 stoichiometry of the complex formation (i.e., n = 1 in Equation (2)) [18,44]. This assumption led to underestimated values of K_a and overestimated values of ΔH , ΔS , and ΔG . Notably, if these parameters are calculated with the assumption of n = 1, they fall within the range of literature values. Furthermore, Zhang L.W. et al. indicated that the values of ΔH and ΔS , derived from affinity capillary electrophoresis data, were significantly lower than those obtained through fluorescence spectroscopy, as displayed in Table 5.

HSA and LV+CD Inclusion Complex Interactions

At 25 °C, the binding constant (K_a) for the ternary system involving HSA and LV+HPCD was five-fold higher than that observed for the binary system of HSA and LV alone. This substantial increase indicates that the hydroxyl group within the HPCD substituent contributes additional hydrogen interactions with the albumin's surface, resulting in the stabilization of the HSA+(LV+HPCD) complex. Furthermore, the pronounced reduction in both ΔH (by approximately 4 times) and ΔS (by approximately 8.5 times) in comparison to the binary system underscores the heightened role of hydrogen interactions in the formation of the HSA+(LV+HPCD) complex (Figure 8).

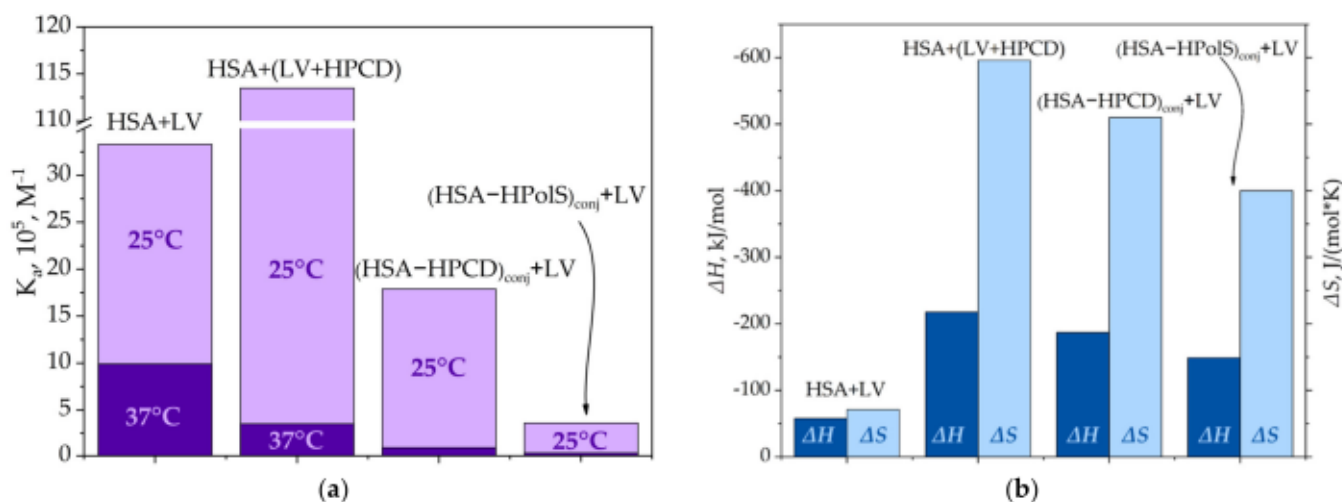


Figure 8. (a) The binding constants for HSA+LV, HSA+HPCD, (HSA-HPolS)_{conj}+LV, and (HSA-HPolS)_{conj}+LV at 25 and 37 °C, PBS, pH 7.4; (b) The thermodynamic parameters for HSA+LV, HSA+HPCD, (HSA-HPolS)_{conj}+LV, and (HSA-HPolS)_{conj}+LV, PBS, pH 7.4.

Similar to the interaction of free LV, the binding constant (K_a) decreased as the temperature rose when HSA interacted with the LV+HPCD complex. However, this effect was significantly more pronounced in the ternary system. In fact, as the temperature increased from 25 to 37 °C, K_a decreased by 30 times. This outcome implies that the LV+HPCD, which possesses a larger molecular size compared to the free drug, is less capable of penetrating the hydrophobic binding pockets of HSA. Consequently, it predominantly interacts with the hydrophilic groups present on the albumin surface. Indeed, in the ternary system, the distance between the donor (HSA) and the fluorescence acceptor (LV+HPCD) increased in comparison to the binary system (Table S2).

(HSA-HPCD)_{conj} and (HSA-HPolS)_{conj} Non-Covalent Interactions with LV

In contrast to the ternary systems, HSA interacted with the LV+HPCD complex. For the conjugates HSA-HPCD or HPolS, the binding constants (K_a) of LV with HSA grafted with CD exhibited consistently lower values across the entire temperature range. Notably, the most significant changes were observed at 37 °C.

For instance, in the case of (HSA-HPCD)_{conj}+LV, the binding constant at 37 °C was determined to be $(9 \pm 1) \times 10^4 \text{ M}^{-1}$, which is 10-fold lower than that observed for the unmodified protein (Table 4). The covalent cross-linking of HSA with HPolS led to an even more pronounced reduction in the interaction constant. In the (HSA+HPolS)_{conj}+LV system, K_a was measured at $(3.1 \pm 1.3) \times 10^4 \text{ M}^{-1}$, representing a 30-fold decrease compared to HSA+LV (Figure 8a,b).

Our explanation is that the toroidal structures of HPCD, anchored to the HSA surface, impede the penetration of LV into the hydrophobic binding sites of HSA, necessitating LV to predominantly interact with the modified HSA surface. Given the profusion of

hydrophilic oligosaccharides adorning the HSA surface, the principal binding forces in these interactions are hydrogen bonds and van der Waals forces.

Notably, the enthalpy change (ΔH) in the cases of (HSA–HPCD)_{conj}+LV and (HSA–HPolS)_{conj}+LV is diminished by factors of 3.2 and 2.5, respectively, relative to HSA+LV. Furthermore, there is a marked reduction in the entropy change (ΔS) by factors of 7 and 5.5 for (HSA–HPCD)_{conj}+LV and (HSA–HPolS)_{conj}+LV, respectively, in comparison to HSA+LV (Figure 8). These phenomena align with the characteristics of systems where the principal driving forces for complex formation are hydrogen bonds and van der Waals forces, as previously elucidated by [51].

Of particular interest, the decline in both enthalpy change (ΔH) and entropy change (ΔS) for systems involving HSA's conjugates is not as pronounced as in the case where LV was encapsulated within the HPCD torus.

Thus, changes in enthalpy and entropy affect drug–protein interactions by influencing the spontaneity and strength of binding. A balance between these two factors determines whether an interaction is thermodynamically favorable. The surface modification of HSA results in a notable reduction in the binding constants. These findings provide valuable insights into the control and modulation of drug carrier properties.

3.4. Kinetics of Levofloxacin Release

To gain insights into the impact of complexation on drug release kinetics, we adopted the equilibrium dialysis method as a model system. This parameter is pivotal for assessing the potential for extended drug release. The formation of drug complexes with cyclodextrin (CD) carriers has been known to exert a nuanced influence on the release rate. For instance, earlier research on ciprofloxacin complexes with β -CD derivatives indicated that complexation correlated with a deceleration in drug release, aligning with the dissociation constants of these complexes [16,21,58].

Our initial focus was to examine the impact on the release rates within binary systems, encompassing non-covalent LV complexes with HPCD, HPolS, and HSA. As anticipated, the formation of the LV+HPCD or LV+HPolS complex led to a decrease in the release rate by 10–20% compared to free LV (Figure 9 and Table 6). This behavior mirrors that of ciprofloxacin when encapsulated in a 3D-matrix system intertwined with covalent complexes of ciprofloxacin with methyl- β -CD via 1,6-hexamethylene diisocyanate [46].

Table 6. Release rates of LV and LV+CD carriers in the absence and presence of HSA¹ with pH 7.4, 37 °C.

	The Presence of HSA	LV	LV+HPCD	LV+HPolS
tg α ²	–	2.4 \pm 0.2	2.2 \pm 0.2	2.9 \pm 0.2
	free	2.1 \pm 0.2	2.2 \pm 0.2	2.9 \pm 0.2
	conjugate ³		2.1 \pm 0.2	2.7 \pm 0.2

¹ Release rates represent the slopes of the initial sections of the LV release curves depicted in Figure 9, reflecting relative changes in concentration per minute at pH 7.4 and 37 °C; ² first 20 min; ³ in these cases, (HSA–HPCD/HPolS)+LV were considered.

In the presence of HSA, a discernible reduction in the release of LV by 15% was observed as compared to free LV. This reduction is in accordance with the (K_{dis}) values. Indeed, LV+HPCD exhibited a K_{dis} of $(1.0 \pm 0.3) \times 10^{-3}$ M, while HSA+LV featured a substantially lower K_{dis} of $(1.0 \pm 0.1) \times 10^{-6}$ M. Consequently, the binding of LV to HSA is notably stronger than its interaction with HPCD, resulting in a diminished release rate for LV in the presence of HSA.

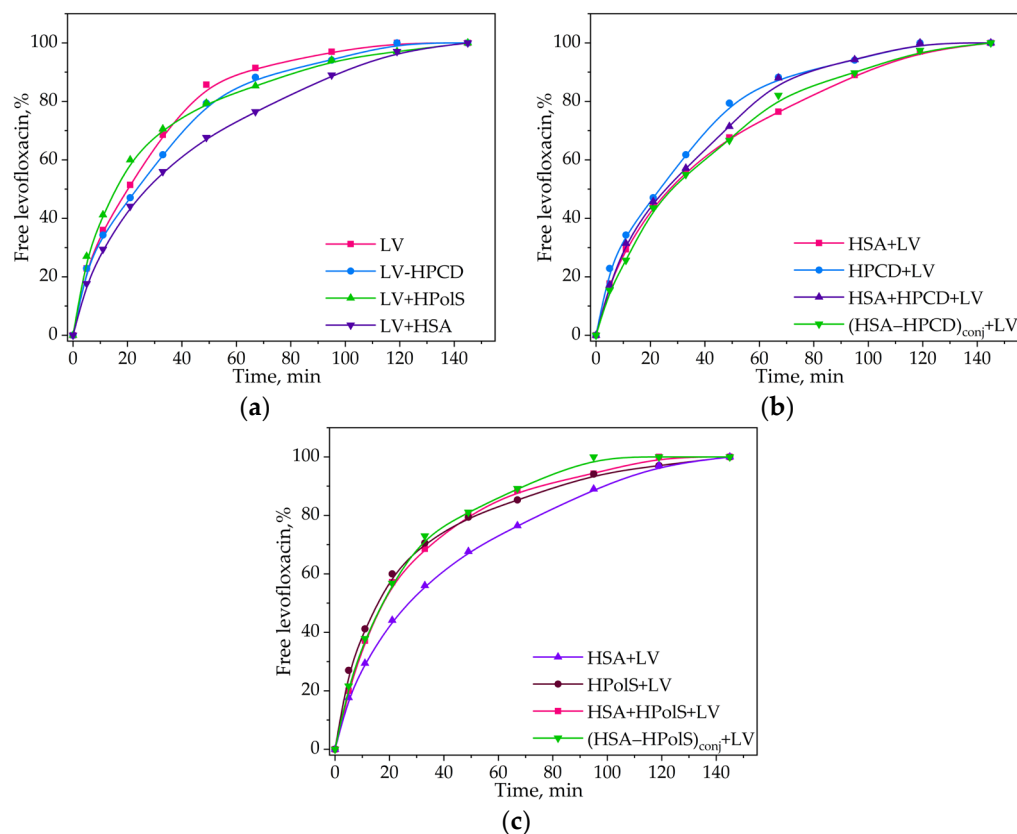


Figure 9. (a) Free LV, LV complex with HPCD (HPCD+LV), LV complex with HpolS (HpolS+LV), and LV complex with HSA (HSA+LV) release curves; (b) HPCD+LV, HSA+LV, LV complex with (HSA–HPCD)_{conj}, and LV+HPCD complex with HSA; (c) HPolS+LV, HSA+LV, LV complex with (HSA–HPolS)_{conj}, and LV+HPolS complex with HSA with $C_{\text{HSA}} = 0.02$ mM, 37 °C, PBS, pH 7.4. All data were obtained in three repetitions and calculated with errors.

Subsequently, we investigated the influence of a ternary system formation on the release rate of LV. Apparently, in systems involving HPolS, we observed a notably higher release rate compared to HSA+LV. Both (HSA–HPolS)_{conj}+LV and HSA+HPolS+LV exhibited nearly identical release rates, both approximately 30% higher than that of HSA+LV (Figure 9c). This phenomenon can be attributed to a 30-fold lower binding constant for (HSA–HPolS)_{conj}+LV compared to HSA+LV.

Interestingly, in systems featuring HPCD, the release rate closely paralleled that of the HSA+LV system, as depicted in the figure. This observation can be attributed to the relatively modest, approximately 10-fold difference in binding constants between (HSA–HPCD)_{conj}+LV and HSA+LV, which is not as pronounced as the difference observed in systems with HPolS (Figure 9b).

3.5. Conjugates Safety

In this investigation, we studied the impact of HSA–HPCD and HSA–HPolS (conjugates without LF) on bacterial cells to ascertain that these conjugates do not possess antibacterial activity. The study utilized the agar well diffusion method—a swift and reliable technique illustrated in Figure 10.

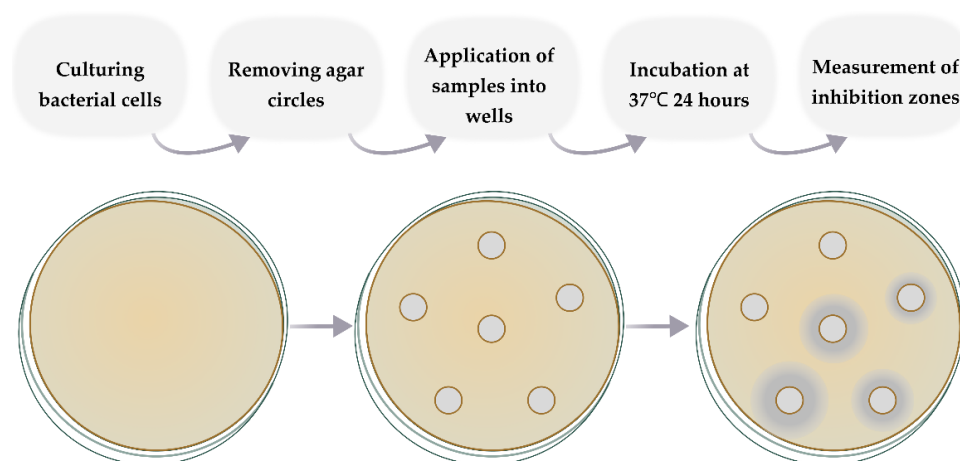


Figure 10. The scheme of the agar well diffusion method.

As it was expected, no inhibition zones were detected on Petri dishes surrounding wells containing solutions of the conjugates (HSA–HPCD and HSA–HPoIS). This observation affirms that HSA_{conj} does not impede the growth of bacterial cultures, even at a high concentration of 5 mg/mL. This outcome aligns with our previous research [21,32], wherein both CDs and HSA exhibited no inhibition zones. The absence of antibacterial activity in these CD-based polymers is not a critical factor in the progression of drug delivery systems, as numerous drug carriers lack inherent antimicrobial properties.

The assessment of materials' blood compatibility, particularly in terms of their potential for hemolysis, is a critical aspect. To estimate the impact of particles on red blood cells, an *in vitro* hemolysis test was conducted using a purified erythrocyte mass isolated from human blood. The classification of biomaterials is based on their hemolysis ratio: non-hemolytic materials exhibiting a ratio of 0–2%, slightly hemolytic in the range of 2–5%, and hemolytic at a ratio of 5–100% [59,60]. In this study, a negative control for 100% hemolysis and a positive control for 0% hemolysis were employed, utilizing Triton X-100 and a saline solution, respectively. This methodology allows for a comprehensive evaluation of the potential adverse effects of materials on red blood cells in a blood environment.

The particles, namely (HSA–HPCD)_{conj}, (HSA–HPoIS)_{conj}, (HSA–LV)_{conj} 1:5, and (HSA–LV)_{conj} 1:10, have demonstrated non-hemolytic characteristics up to a concentration of 3.3 mg/mL. This observation aligns logically with the composition of these particles that are based on HSA, which is a major blood protein. The safety and hemocompatibility exhibited by these particles make them promising candidates for the development of drug formulations for intravenous administration. Biocompatibility is a crucial attribute for drug carriers, and the results from this study support the suitability of these particles for such applications.

In our previous research, we established that HPoIS itself is non-hemolytic up to a concentration of 1.7 mg/mL. Additionally, literature data suggests that certain components of human blood, particularly albumins, play a protective role by significantly mitigating the cytotoxic effects of CDs [61]. This information underscores the potential of the studied particles for safe and effective drug delivery systems, aligning with the protective properties associated with blood components.

3.6. Antibacterial Activity of Conjugates

Nanoparticles constructed from HSA have garnered significant attention due to the numerous advantages associated with HSA. These include biocompatibility, biodegradability, well-established tolerability in human subjects, non-toxic and non-immunogenic attributes, and remarkable stability in various environments [6,62,63].

In this study, we investigated the impact of conjugates with HSA formation on the antibacterial activity of LV. In the case of *Escherichia coli*, Gram-negative bacteria, all of the

studied samples containing LV exhibited a notable reduction in the rate of bacterial growth after 20 h (Figure 11a).

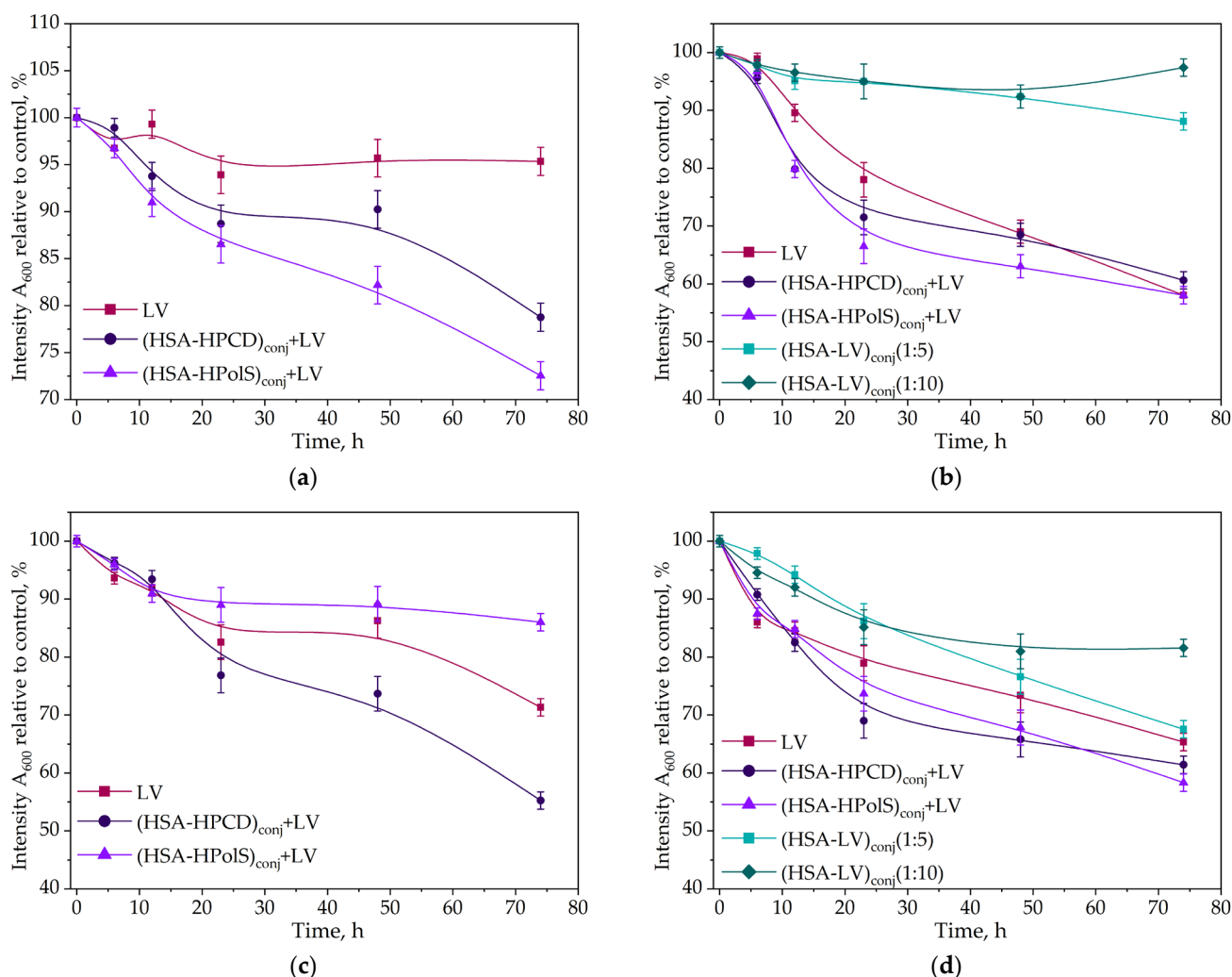


Figure 11. Kinetic curves depicting the dependency of optical absorbance at 600 nm (relative to control) at 37 °C in correlation with the number of colony-forming units (CFU). The curves span the incubation time of 0 to 72 h, focusing on *E. coli* cells treated with antibacterial drugs, specifically C_{LV} at a concentration of 10 ng/mL. (a) $C_{LV} = 50$ ng/mL; (b) for *B. subtilis* cells, $C_{LV} = 10$ ng/mL; (c) for *B. subtilis* cells, $C_{LV} = 50$ ng/mL at 37 °C; (d) All data were obtained in three repetitions and calculated with errors.

The most potent inhibitory effect was observed in the system featuring a non-covalent complex of LV with the HSA grafted with polymeric CD (HSA-HPolS)_{conj}. These pronounced changes were particularly noticeable at LV concentration of 10 ng/mL. Remarkably, (HSA-HPolS)_{conj}+LV at this concentration displayed 40% higher activity compared to free LV at the same concentration level. For monomeric CD, (HSA-HPCD)_{conj}+LV demonstrated a 30% increase in antibacterial activity relative to free LV (Figure 11a,b).

Subsequent testing of the samples at a higher LV concentration (50 ng/mL) revealed significant inhibitory effects across all formulations (Figure 12 and Table 7). The covalent conjugate HSA with LV (HSA-LV 1:10)_{conj} and (HSA-LV 1:5)_{conj} displayed a marginal reduction in activity, comparable to that at 10 ng/mL LV system. This observation can be attributed to the reduced availability of free LV in the HSA-LV systems in comparison to other systems where LV was not covalently linked (Figure 11b).

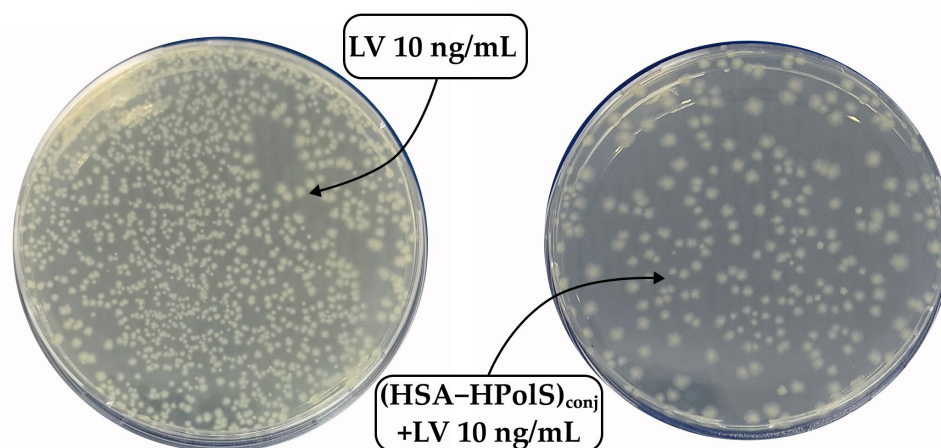


Figure 12. The Petri dishes were seeded with a solution of *Escherichia coli* cells diluted 10^6 times. LV was added to one dish at a concentration of 50 ng/mL, and (HSA+HPolS)_{conj}+LV was added to another dish at the same concentration. Incubation was carried out at 37 °C for 24 h.

Table 7. The number of colony-forming units (CFU) in the cells’ suspension with antibacterial agents (in all samples, the LV concentration was maintained 50 ng/mL).

Strain	Time, h	10^9 CFU ¹				
		LV	(HSA – HPCD) _{conj} +LV	(HSA – HPolS) _{conj} +LV	HSA – LV 1:5	HSA – LV 1:10
<i>E. coli</i>	24	1.6 ± 0.2	2.0 ± 0.2	0.2 ± 0.2	1.0 ± 0.1	1.1 ± 0.1
	48	2.1 ± 0.2	2.3 ± 0.2	0.7 ± 0.1	1.7 ± 0.2	1.6 ± 0.1
<i>B. subtilis</i>	24	0.9 ± 0.1	0.4 ± 0.1	0.8 ± 0.1	0.45 ± 0.05	1.1 ± 0.1
	48	1.0 ± 0.1	0.5 ± 0.1	0.9 ± 0.1	0.51 ± 0.05	1.2 ± 0.1

¹ In this experiment, the cells were treated with antibacterial agents, and the number of CFUs was determined by counting the colonies that grew on Petri dishes after incubation. The incubation was carried out at 37 °C for 24–48 h. All data were obtained in three repetitions.

Further, we conducted similar experiments with Gram+ bacteria *Bacillus Subtilis*, yielding intriguing results. Firstly, we noted that HSA – LV exhibited comparable activity to (HSA – HPolS)_{conj}+LV (Figure 11c,d), in contrast to the findings with *E. coli*. This discrepancy is likely associated with the fact that *B. subtilis* forms robust biofilms, hindering the penetration of LV into bacterial cells and thereby limiting its antibacterial properties [64].

We determined the minimum inhibition concentration (MIC) values for LV, (HSA – HPCD)_{conj}+LV, (HSA – HPolS)_{conj}+LV, (HSA – LV)_{conj} 1:5, and (HSA – LV)_{conj} 1:10 (Table 8) using the agar diffusion method (Figures 10 and 13). The MIC for free LV was 1.3 µg/mL and 0.9 µg/mL for *E. coli* and *B. subtilis*, respectively. Interestingly, in the case of *E. coli*, complexation of LV with grafted HSA did not result in a decrease in MIC values. However, covalent binding of LV with HSA led to an increase in MIC up to 9 µg/mL. These findings align well with the antibacterial activity observed in liquid media (Figure 11).

Table 8. Minimum inhibition concentration (MIC) values (µg/mL) determined under conditions of pH at 7.4 using a PBS sterile buffer and employing the agar well diffusion method at 37 °C for 24 h.

Strain	LV	(HSA – HPCD) _{conj} +LV	(HSA – HPolS) _{conj} +LV	(HSA – LV) _{conj} 1:5	(HSA – LV) _{conj} 1:10
<i>E. coli</i> ATCC 25922	1.3 ± 0.1	1.3 ± 0.1	1.3 ± 0.1	9 ± 1	9 ± 1
<i>B. subtilis</i> ATCC 6633	0.9 ± 0.1	0.7 ± 0.1	0.8 ± 0.1	3 ± 1	5 ± 1

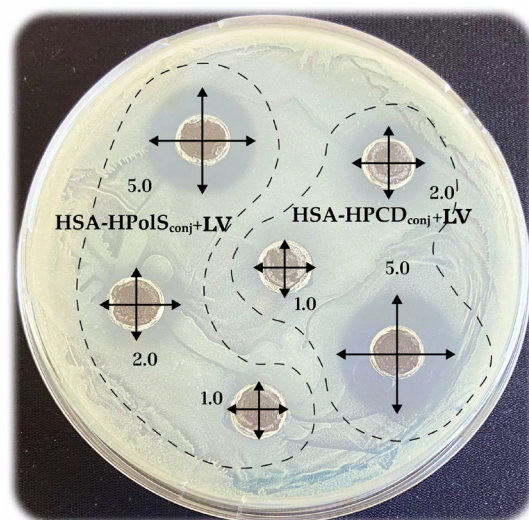


Figure 13. The results for the antibacterial activity of $(\text{HSA-HPCD})_{\text{conj}}+\text{LV}$ and $(\text{HSA-HPolS})_{\text{conj}}+\text{LV}$; C_{LV} is 1.0–5.0 $\mu\text{g/mL}$, 37 °C, agar-well diffusion method, *B. subtilis*.

For *B. subtilis*, complexation of LV with grafted HSA resulted in a slight decrease in MIC values to 0.7 $\mu\text{g/mL}$, whereas covalent binding of LV with HSA increased MIC to 3 mg/mL . Again, these results correlate with the antibacterial activity observed in liquid media (Figure 11).

Within this context, the conjugation of LV with HSA serves as an antiadherent compound, potentially inhibiting the formation of biofilms. This, in turn, significantly contributes to the enhanced antibacterial activity of HSA–LV conjugates. Furthermore, in the case of *B. subtilis*, $(\text{HSA-HPCD})_{\text{conj}}+\text{LV}$ emerges as the most effective drug carrier.

In the realm of antibacterial activity, the strategy of preventing biofilm formation on non-living surfaces has yielded varied outcomes [65–68]. Significantly, certain proteins have shown the ability to reduce bacterial biofilm formation on non-living surfaces, rendering these surfaces less hydrophobic [65,69–71]. Moreover, there is a wealth of information underscoring the advantageous influence of HSA in this context.

In addition to conjugates for antibacterial activity, conjugates with albumin are also promising for creating formulations for cytostatic drugs. So, the research of Kinoshita and colleagues has demonstrated the potential of HSA–doxorubicin conjugates in tumor treatment compared to free doxorubicin [72], where tumor cells actively utilize endogenous HSA as a source of amino acids to support their rapid proliferation, facilitated by HSA receptors such as gp60 or SPARC [73].

4. Conclusions

The novel drug delivery systems for Levofloxacin (LV)-based HSA grafted with monomeric or polymeric HPCD is suggested. We developed three HSA-based particles: HSA–LV conjugate, the non-covalent complexes of LV with HSA conjugated with cyclodextrins (HSA–HPCD) and with polymeric cyclodextrins (HSA–HPolS). We employed FTIR-spectroscopy to confirm the structural characteristics of these conjugates. In the case of HSA–LV conjugates, we observed an increase in the intensity of the amide I and amide II bands, indicative of changes in the protein’s secondary structure. Additionally, for $(\text{HSA-HPCD})_{\text{conj}}$ and $(\text{HSA-HPolS})_{\text{conj}}$, we detected distinctive bands corresponding to urethane bonds in the FTIR spectra.

The $\text{CD}(\text{polymers})\text{-LV}$ association constant is two to three orders of magnitude higher than that of HSA+LV . So, we engrafted monomeric or polymeric CDs on the surface of HSA molecules to strengthen the LV adsorption on HSA. Our primary objective was gaining insights into the interactions between LV and the $(\text{HSA-HPCD})_{\text{conj}}$ and $(\text{HSA-HPolS})_{\text{conj}}$ systems. Through fluorescence quenching experiments, we determined the binding constants (K_d) for $\text{LV}+(\text{HSA-HPCD})_{\text{conj}}$ and $\text{LV}+(\text{HSA-HPolS})_{\text{conj}}$ to be $(9 \pm 1) \times 10^4 \text{ M}^{-1}$

and $(3.1 \pm 1.3) \times 10^4 \text{ M}^{-1}$, respectively. The thermodynamic parameters, ΔH and ΔS , of the LV and $(\text{HSA}-\text{HPCD})_{\text{conj}}/(\text{HSA}-\text{HPolS})_{\text{conj}}$ complex formations were determined, revealing that hydrogen bonds and van der Waals interactions play a significant role in complex formation.

Furthermore, we explored the impact of these HSA grafted by CDs conjugates on the antibacterial properties of LV. We have found that $\text{LV}+(\text{HSA}-\text{HPolS})_{\text{conj}}$ exhibited the highest antibacterial activity against *E. coli* (showing 40% higher activity compared to free LV), whereas $\text{LV}+(\text{HSA}-\text{HPCD})_{\text{conj}}$ was the most effective against *B. subtilis*. Both HSA conjugates were more potent than LV alone or LV with HSA.

Further fine-tuning of HSA could yield an improvement in biodistribution and thus, a more favorable risk/benefit ratio.

Supplementary Materials: The following supporting information can be downloaded at: <https://www.mdpi.com/article/10.3390/futurepharmacol4010010/s1>, Table S1. Temperature dependence of the Stern-Volmer quenching constants for the LV-HSA's systems. Table S2. Energy transfer parameters for the interactions of the drugs with human serum albumin (25 °C, PBS, pH 7.4).

Author Contributions: Conceptualization: T.Y.K., L.R.Y. and E.V.K.; Experimental work, data analysis and interpretation: T.Y.K., L.R.Y. and E.V.K.; methodology of microbiological experiments, N.G.B.; Writing—Original draft preparation: T.Y.K. and L.R.Y.; Writing—Review and editing: T.Y.K., L.R.Y. and E.V.K.; Supervision: E.V.K. All authors have read and agreed to the published version of the manuscript.

Funding: This work was supported by the Russian Science Foundation grant number 22-24-00604.

Institutional Review Board Statement: Not applicable.

Informed Consent Statement: Not applicable.

Data Availability Statement: All data obtained or analyzed in the course of this study are included in this published article and its Supplementary Materials.

Acknowledgments: The work was performed using the equipment (FTIR microscope MICRAN-3, FTIR spectrometer Bruker Tensor 27, Jasco J-815 CD Spectrometer, AFM microscope NTEGRA II) of the program for the development of Moscow State University.

Conflicts of Interest: The authors declare no conflicts of interest.

References

1. Zheng, Y.-R.; Suntharalingam, K.; Johnstone, T.C.; Yoo, H.; Lin, W.; Brooks, J.G.; Lippard, S.J. Pt(IV) Prodrugs Designed to Bind Non-Covalently to Human Serum Albumin for Drug Delivery. *J. Am. Chem. Soc.* **2014**, *136*, 8790–8798. [[CrossRef](#)] [[PubMed](#)]
2. Bohnert, T.; Gan, L.-S. Plasma protein binding: From discovery to development. *J. Pharm. Sci.* **2013**, *102*, 2953–2994. [[CrossRef](#)]
3. Fanali, G.; di Masi, A.; Trezza, V.; Marino, M.; Fasano, M.; Ascenzi, P. Human serum albumin: From bench to bedside. *Mol. Asp. Med.* **2012**, *33*, 209–290. [[CrossRef](#)] [[PubMed](#)]
4. Yang, F.; Zhang, Y.; Liang, H. Interactive association of drugs binding to human serum albumin. *Int. J. Mol. Sci.* **2014**, *15*, 3580–3595. [[CrossRef](#)] [[PubMed](#)]
5. Trotta, F.; Caldera, F.; Cavalli, R.; Soster, M.; Riedo, C.; Biasizzo, M.; Uccello Barretta, G.; Balzano, F.; Brunella, V. Molecularly imprinted cyclodextrin nanospheres for the controlled delivery of L-DOPA: Perspectives for the treatment of Parkinson's disease. *Expert Opin. Drug Deliv.* **2016**, *13*, 1671–1680. [[CrossRef](#)] [[PubMed](#)]
6. Kratz, F. Albumin as a drug carrier: Design of prodrugs, drug conjugates and nanoparticles. *J. Control. Release* **2008**, *132*, 171–183. [[CrossRef](#)] [[PubMed](#)]
7. Kratochwil, N.A.; Huber, W.; Müller, F.; Kansy, M.; Gerber, P.R. Predicting plasma protein binding of drugs: A new approach. *Biochem. Pharmacol.* **2002**, *64*, 1355–1374. [[CrossRef](#)]
8. Davis, R.; Bryson, H.M. Levofloxacin. *Drugs* **1994**, *47*, 677–700. [[CrossRef](#)]
9. Van Bambeke, F.; Michot, J.M.; Van Eldere, J.; Tulkens, P.M. Quinolones in 2005: An update. *Clin. Microbiol. Infect.* **2005**, *11*, 256–280. [[CrossRef](#)]
10. Wolfson, J.S.; Hooper, D.C. Fluoroquinolone antimicrobial agents. *Clin. Microbiol. Rev.* **1989**, *2*, 378–424. [[CrossRef](#)]
11. Tiwari, G.; Tiwari, R.; Bannerjee, S.; Bhati, L.; Pandey, S.; Pandey, P.; Sriwastawa, B. Drug delivery systems: An updated review. *Int. J. Pharm. Investig.* **2012**, *2*, 2. [[CrossRef](#)] [[PubMed](#)]
12. Davis, M.E.; Brewster, M.E. Cyclodextrin-based pharmaceuticals: Past, present and future. *Nat. Rev. Drug Discov.* **2004**, *3*, 1023–1035. [[CrossRef](#)] [[PubMed](#)]
13. Stella, V.J.; He, Q. Cyclodextrins. *Toxicol. Pathol.* **2008**, *36*, 30–42. [[CrossRef](#)] [[PubMed](#)]

14. Le-Deygen, I.M.; Skuredina, A.A.; Uporov, I.V.; Kudryashova, E.V. Thermodynamics and molecular insight in guest–host complexes of fluoroquinolones with β -cyclodextrin derivatives, as revealed by ATR-FTIR spectroscopy and molecular modeling experiments. *Anal. Bioanal. Chem.* **2017**, *409*, 6451–6462. [[CrossRef](#)] [[PubMed](#)]
15. Yakupova, L.R.; Skuredina, A.A.; Markov, P.O.; Le-Deygen, I.M.; Kudryashova, E.V. Cyclodextrin Polymers as a Promising Drug Carriers for Stabilization of Meropenem Solutions. *Appl. Sci.* **2023**, *13*, 3608. [[CrossRef](#)]
16. Skuredina, A.A.; Yakupova, L.R.; Kopnova, T.Y.; Le-Deygen, I.M.; Belogurova, N.G.; Kudryashova, E.V. Cyclodextrins and Their Polymers Affect Human Serum Albumin’s Interaction with Drugs Used in the Treatment of Pulmonary Infections. *Pharmaceutics* **2023**, *15*, 1598. [[CrossRef](#)] [[PubMed](#)]
17. Varshney, A.; Sen, P.; Ahmad, E.; Rehan, M.; Subbarao, N.; Khan, R.H. Ligand Binding Strategies of Human Serum Albumin: How Can the Cargo be Utilized? *Chirality* **2010**, *22*, 77–87. [[CrossRef](#)] [[PubMed](#)]
18. Zhang, L.-W.; Wang, K.; Zhang, X.-X. Study of the interactions between fluoroquinolones and human serum albumin by affinity capillary electrophoresis and fluorescence method. *Anal. Chim. Acta* **2007**, *603*, 101–110. [[CrossRef](#)]
19. Missoun, F.; de los Ríos, A.P.; Ortiz-Martínez, V.; Salar-García, M.J.; Hernández-Fernández, J.; Hernández-Fernández, F.J. Discovering Low Toxicity Ionic Liquids for *Saccharomyces cerevisiae* by Using the Agar Well Diffusion Test. *Processes* **2020**, *8*, 1163. [[CrossRef](#)]
20. Le-Deygen, I.M.; Skuredina, A.A.; Mamaeva, P.V.; Kolmogorov, I.M.; Kudryashova, E.V. Conjugates of Chitosan with β -Cyclodextrins as Promising Carriers for the Delivery of Levofloxacin: Spectral and Microbiological Studies. *Life* **2023**, *13*, 272. [[CrossRef](#)]
21. Skuredina, A.A.; Kopnova, T.Y.; Tychinina, A.S.; Golyshev, S.A.; Le-Deygen, I.M.; Belogurova, N.G.; Kudryashova, E.V. The New Strategy for Studying Drug-Delivery Systems with Prolonged Release: Seven-Day In Vitro Antibacterial Action. *Molecules* **2022**, *27*, 8026. [[CrossRef](#)]
22. Hearn, M.T.W. 1,1'-Carbonyldiimidazole-mediated immobilization of enzymes and affinity ligands. *Methods Enzymol.* **1987**, *135*, 102–117.
23. Métro, T.-X.; Martínez, J.; Lamaty, F. 1,1'-Carbonyldiimidazole and Mechanochemistry: A Shining Green Combination. *ACS Sustain. Chem. Eng.* **2017**, *5*, 9599–9602. [[CrossRef](#)]
24. Stöllner, D.; Scheller, F.W.; Warsinke, A. Activation of Cellulose Membranes with 1,1'-Carbonyldiimidazole or 1-Cyano-4-dimethylaminopyridinium tetrafluoroborate as a Basis for the Development of Immunosensors. *Anal. Biochem.* **2002**, *304*, 157–165. [[CrossRef](#)] [[PubMed](#)]
25. Faridnouri, H.; Ghouchian, H.; Hashemnia, S. Direct electron transfer enhancement of covalently bound tyrosinase to glassy carbon via Woodward’s reagent K. *Bioelectrochemistry* **2011**, *82*, 1–9. [[CrossRef](#)] [[PubMed](#)]
26. Puri, R.N.; Colman, R.W. A Novel Method for Chemical Modification of Functional Groups Other Than a Carboxyl Group in Proteins by N-Ethyl-5-phenylisooxazolium-3'-sulfonate (Woodward’s Reagent-K): Inhibition of ADP-Induced Platelet Responses Involves Covalent Modification of Aggreg. *Anal. Biochem.* **1996**, *240*, 251–261. [[CrossRef](#)] [[PubMed](#)]
27. Dobryakova, N.V.; Zhdanov, D.D.; Sokolov, N.N.; Aleksandrova, S.S.; Pokrovskaya, M.V.; Kudryashova, E.V. Rhodospirillum rubrum L-Asparaginase Conjugates with Polyamines of Improved Biocatalytic Properties as a New Promising Drug for the Treatment of Leukemia. *Appl. Sci.* **2023**, *13*, 3373. [[CrossRef](#)]
28. Paoli, P.; Fiaschi, T.; Cirri, P.; Camici, G.; Manao, G.; Cappugi, G.; Raugei, G.; Moneti, G.; Ramponi, G. Mechanism of acylphosphatase inactivation by Woodward’s reagent K. *Biochem. J.* **1997**, *328*, 855–861. [[CrossRef](#)] [[PubMed](#)]
29. Sinha, U.; Brewer, J.M. A spectrophotometric method for quantitation of carboxyl group modification of proteins using Woodward’s Reagent K. *Anal. Biochem.* **1985**, *151*, 327–333. [[CrossRef](#)]
30. Dunn, B.M.; Anfinsen, C.B.; Shrager, R.I. Kinetics of Woodward’s Reagent K Hydrolysis and Reaction with Staphylococcal Nuclease. *J. Biol. Chem.* **1974**, *249*, 3717–3723. [[CrossRef](#)]
31. Skuredina, A.A.; Le-Deygen, I.M.; Belogurova, N.G.; Kudryashova, E.V. Effect of cross-linking on the inclusion complex formation of derivatized β -cyclodextrins with small-molecule drug moxifloxacin. *Carbohydr. Res.* **2020**, *498*, 108183. [[CrossRef](#)]
32. Yakupova, L.R.; Kopnova, T.Y.; Skuredina, A.A.; Le-Deygen, I.M.; Shustrov, P.N.; Novoselov, A.M.; Kudryashova, E.V. The Formation of β -Cyclodextrin Complexes with Levofloxacin and Ceftriaxone as an Approach to the Regulation of Drugs’ Pharmacokinetic. *Colloid J.* **2023**, *85*, 114–127. [[CrossRef](#)]
33. Richner, G.; Puxty, G. Assessing the Chemical Speciation during CO₂ Absorption by Aqueous Amines Using in Situ FTIR. *Ind. Eng. Chem. Res.* **2012**, *51*, 14317–14324. [[CrossRef](#)]
34. Furer, V.L.; Vandyukova, I.I.; Vandyukov, A.E.; Fuchs, S.; Majoral, J.P.; Caminade, A.M.; Kovalenko, V.I. Vibrational spectra study of fluorescent dendrimers built from the cyclotriphosphazene core with terminal dansyl and carbamate groups. *Spectrochim. Acta Part A Mol. Biomol. Spectrosc.* **2011**, *79*, 462–470. [[CrossRef](#)]
35. Lingegowda, D.C.; Kumar, J.K.; Prasad, A.D.; Zarei, M.; Gopal, S. FTIR spectroscopic studies on cleome gynandra-Comparative analysis of functional group before and after extraction. *Rom. J. Biophys.* **2012**, *22*, 137–143.
36. Tretiakova, D.; Le-Deigen, I.; Onishchenko, N.; Kuntsche, J.; Kudryashova, E.; Vodovozova, E. Phosphatidylinositol Stabilizes Fluid-Phase Liposomes Loaded with a Melphalan Lipophilic Prodrug. *Pharmaceutics* **2021**, *13*, 473. [[CrossRef](#)] [[PubMed](#)]
37. Dong, A.; Meyer, J.D.; Brown, J.L.; Manning, M.C.; Carpenter, J.F. Comparative fourier transform infrared and circular dichroism spectroscopic analysis of α 1-proteinase inhibitor and ovalbumin in aqueous solution. *Arch. Biochem. Biophys.* **2000**, *383*, 148–155. [[CrossRef](#)] [[PubMed](#)]
38. Haris, P.I.; Severcan, F. FTIR spectroscopic characterization of protein structure in aqueous and non-aqueous media. *J. Mol. Catal. B Enzym.* **1999**, *7*, 207–221. [[CrossRef](#)]

39. Aleem, O.; Kuchekar, B.; Pore, Y.; Late, S. Effect of β -cyclodextrin and hydroxypropyl β -cyclodextrin complexation on physico-chemical properties and antimicrobial activity of cefdinir. *J. Pharm. Biomed. Anal.* **2008**, *47*, 535–540. [[CrossRef](#)]
40. Zhao, D.; Zhao, L.; Zhu, C.-S.; Huang, W.-Q.; Hu, J.-L. Water-insoluble β -cyclodextrin polymer crosslinked by citric acid: Synthesis and adsorption properties toward phenol and methylene blue. *J. Incl. Phenom. Macrocycl. Chem.* **2009**, *63*, 195–201. [[CrossRef](#)]
41. Iranfar, H.; Rajabi, O.; Salari, R.; Chamani, J. Probing the Interaction of Human Serum Albumin with Ciprofloxacin in the Presence of Silver Nanoparticles of Three Sizes: Multispectroscopic and ζ Potential Investigation. *J. Phys. Chem. B* **2012**, *116*, 1951–1964. [[CrossRef](#)]
42. Zhang, H.-M.; Wang, Y.-Q.; Jiang, M.-L. A fluorimetric study of the interaction of C.I. Solvent Red 24 with haemoglobin. *Dye. Pigment.* **2009**, *82*, 156–163. [[CrossRef](#)]
43. Wei, Y.; Li, J.; Dong, C.; Shuang, S.; Liu, D.; Huie, C.W. Investigation of the association behaviors between biliverdin and bovine serum albumin by fluorescence spectroscopy. *Talanta* **2006**, *70*, 377–382. [[CrossRef](#)]
44. Seedher, N.; Agarwal, P. Complexation of fluoroquinolone antibiotics with human serum albumin: A fluorescence quenching study. *J. Lumin.* **2010**, *130*, 1841–1848. [[CrossRef](#)]
45. Kaur, A.; Khan, I.A.; Banipal, P.K.; Banipal, T.S. Deciphering the complexation process of a fluoroquinolone antibiotic, levofloxacin, with bovine serum albumin in the presence of additives. *Spectrochim. Acta Part A Mol. Biomol. Spectrosc.* **2018**, *191*, 259–270. [[CrossRef](#)]
46. Skuredina, A.A.; Kopnova, T.Y.; Belogurova, N.G.; Kudryashova, E.V. Encapsulation of Ciprofloxacin into a Cyclodextrin Polymer Matrix: The Complex Formation with Human Serum Albumin and In Vitro Studies. *Chemistry* **2023**, *5*, 1942–1960. [[CrossRef](#)]
47. Yakupova, L.R.; Kopnova, T.Y.; Skuredina, A.A.; Kudryashova, E.V. Effect of Methyl- β -Cyclodextrin on the Interaction of Fluoroquinolones with Human Serum Albumin. *Russ. J. Bioorg. Chem.* **2022**, *48*, 163–172. [[CrossRef](#)]
48. Yakupova, L.R.; Skuredina, A.A.; Kopnova, T.Y.; Kudryashova, E.V. In Vitro Biological Properties of Cyclodextrin-Based Polymers: Interaction with Human Serum Albumin, Red Blood Cells and Bacteria. *Polysaccharides* **2023**, *4*, 343–357. [[CrossRef](#)]
49. Hu, Y.J.; Ou-Yang, Y.; Zhang, Y.; Liu, Y. Affinity and specificity of ciprofloxacin-bovine serum albumin interactions: Spectroscopic approach. *Protein J.* **2010**, *29*, 234–241. [[CrossRef](#)]
50. Rehman, M.T.; Shamsi, H.; Khan, A.U. Insight into the binding mechanism of imipenem to human serum albumin by spectroscopic and computational approaches. *Mol. Pharm.* **2014**, *11*, 1785–1797. [[CrossRef](#)]
51. Ross, P.D.; Subramanian, S. Thermodynamics of Protein Association Reactions: Forces Contributing to Stability. *Biochemistry* **1981**, *20*, 3096–3102. [[CrossRef](#)]
52. Seedher, N.; Agarwal, P. Competitive binding of fluoroquinolone antibiotics and some other drugs to human serum albumin: A luminescence spectroscopic study. *Luminescence* **2013**, *28*, 562–568. [[CrossRef](#)]
53. Poureshghi, F.; Ghandforoushan, P.; Safarnejad, A.; Soltani, S. Interaction of an antiepileptic drug, lamotrigine with human serum albumin (HSA): Application of spectroscopic techniques and molecular modeling methods. *J. Photochem. Photobiol. B Biol.* **2017**, *166*, 187–192. [[CrossRef](#)]
54. Paul, B.K.; Guchhait, N. A spectral deciphering of the binding interaction of an intramolecular charge transfer fluorescence probe with a cationic protein: Thermodynamic analysis of the binding phenomenon combined with blind docking study. *Photochem. Photobiol. Sci.* **2011**, *10*, 980–991. [[CrossRef](#)]
55. Zhang, G.; Ma, Y. Mechanistic and conformational studies on the interaction of food dye amaranth with human serum albumin by multispectroscopic methods. *Food Chem.* **2013**, *136*, 442–449. [[CrossRef](#)]
56. Paul, B.K.; Guchhait, N.; Bhattacharya, S.C. Binding of ciprofloxacin to bovine serum albumin: Photophysical and thermodynamic aspects. *J. Photochem. Photobiol. B Biol.* **2017**, *172*, 11–19. [[CrossRef](#)]
57. Tabassum, S.; Al-Asbahy, W.M.; Afzal, M.; Arjmand, F. Synthesis, characterization and interaction studies of copper based drug with Human Serum Albumin (HSA): Spectroscopic and molecular docking investigations. *J. Photochem. Photobiol. B Biol.* **2012**, *114*, 132–139. [[CrossRef](#)]
58. Skuredina, A.A.; Kopnova, T.Y.; Le-deygen, I.M.; Kudryashova, E. V Physical and Chemical Properties of the Guest–Host Inclusion Complexes of Cyprofloxacin with β -Cyclodextrin Derivatives. *Mosc. Univ. Chem. Bull.* **2020**, *75*, 218–224. [[CrossRef](#)]
59. Sahiner, N.; Sagbas, S.; Sahiner, M.; Blake, D.A.; Reed, W.F. Polydopamine particles as nontoxic, blood compatible, antioxidant and drug delivery materials. *Colloids Surf. B Biointerfaces* **2018**, *172*, 618–626. [[CrossRef](#)]
60. Sahiner, N.; Sagbas, S.; Aktas, N. Preparation of macro-, micro-, and nano-sized poly(Tannic acid) particles with controllable degradability and multiple biomedical uses. *Polym. Degrad. Stab.* **2016**, *129*, 96–105. [[CrossRef](#)]
61. Szente, L.; Singhal, A.; Domokos, A.; Song, B. Cyclodextrins: Assessing the Impact of Cavity Size, Occupancy, and Substitutions on Cytotoxicity and Cholesterol Homeostasis. *Molecules* **2018**, *23*, 1228. [[CrossRef](#)]
62. Sparreboom, A.; Scripture, C.D.; Trieu, V.; Williams, P.J.; De, T.; Yang, A.; Beals, B.; Figg, W.D.; Hawkins, M.; Desai, N. Comparative Preclinical and Clinical Pharmacokinetics of a Cremophor-Free, Nanoparticle Albumin-Bound Paclitaxel (ABI-007) and Paclitaxel Formulated in Cremophor (Taxol). *Clin. Cancer Res.* **2005**, *11*, 4136–4143. [[CrossRef](#)] [[PubMed](#)]
63. Chemmanur, A.T.; Wu, G.Y. Drug evaluation: Albuferon-alpha—an antiviral interferon-alpha/albumin fusion protein. *Curr. Opin. Investig. Drugs* **2006**, *7*, 750–758. [[PubMed](#)]
64. Arnaouteli, S.; Bamford, N.C.; Stanley-Wall, N.R.; Kovács, Á.T. Bacillus subtilis biofilm formation and social interactions. *Nat. Rev. Microbiol.* **2021**, *19*, 600–614. [[CrossRef](#)] [[PubMed](#)]
65. An, Y.H.; Friedman, R.J. Concise review of mechanisms of bacterial adhesion to biomaterial surfaces. *J. Biomed. Mater. Res.* **1998**, *43*, 338–348. [[CrossRef](#)]

66. Bridgett, M.J.; Davies, M.C.; Denyer, S.P. Control of staphylococcal adhesion to polystyrene surfaces by polymer surface modification with surfactants. *Biomaterials* **1992**, *13*, 411–416. [[CrossRef](#)] [[PubMed](#)]
67. Donlan, R.M.; Costerton, J.W. Biofilms: Survival Mechanisms of Clinically Relevant Microorganisms. *Clin. Microbiol. Rev.* **2002**, *15*, 167–193. [[CrossRef](#)]
68. Paulsson, M.; Kober, M.; Freij-Larsson, C.; Stollenwerk, M.; Wesslén, B.; Ljungh, Å. Adhesion of staphylococci to chemically modified and native polymers, and the influence of preadsorbed fibronectin, vitronectin and fibrinogen. *Biomaterials* **1993**, *14*, 845–853. [[CrossRef](#)]
69. Brokke, P.; Dankert, J.; Carballo, J.; Feijen, J. Adherence of Coagulase-Negative Staphylococci onto Polyethylene Catheters in vitro and in vivo: A Study on the Influence of various Plasma Proteins. *J. Biomater. Appl.* **1991**, *5*, 204–226. [[CrossRef](#)]
70. Reynolds, E.C.; Wong, A. Effect of adsorbed protein on hydroxyapatite zeta potential and Streptococcus mutans adherence. *Infect. Immun.* **1983**, *39*, 1285–1290. [[CrossRef](#)]
71. del Prado, G.; Ruiz, V.; Naves, P.; Rodríguez-Cerrato, V.; Soriano, F.; del Carmen Ponte, M. Biofilm formation by Streptococcus pneumoniae strains and effects of human serum albumin, ibuprofen, N-acetyl-l-cysteine, amoxicillin, erythromycin, and levofloxacin. *Diagn. Microbiol. Infect. Dis.* **2010**, *67*, 311–318. [[CrossRef](#)] [[PubMed](#)]
72. Kinoshita, R.; Ishima, Y.; Chuang, V.T.G.; Watanabe, H.; Shimizu, T.; Ando, H.; Okuhira, K.; Otagiri, M.; Ishida, T.; Maruyama, T. The Therapeutic Effect of Human Serum Albumin Dimer-Doxorubicin Complex against Human Pancreatic Tumors. *Pharmaceutics* **2021**, *13*, 1209. [[CrossRef](#)] [[PubMed](#)]
73. Desai, N.; Trieu, V.; Damascelli, B.; Soon-Shiong, P. SPARC Expression Correlates with Tumor Response to Albumin-Bound Paclitaxel in Head and Neck Cancer Patients. *Transl. Oncol.* **2009**, *2*, 59–64. [[CrossRef](#)] [[PubMed](#)]

Disclaimer/Publisher’s Note: The statements, opinions and data contained in all publications are solely those of the individual author(s) and contributor(s) and not of MDPI and/or the editor(s). MDPI and/or the editor(s) disclaim responsibility for any injury to people or property resulting from any ideas, methods, instructions or products referred to in the content.